8.09 Waves in the Core and Mechanical Core–Mantle Interactions

D Jault, University Grenoble Alpes/CNRS, Grenoble, France
CC Finlay, DTU Space, Technical University of Denmark, Lyngby, Denmark

8.09.1 Motivation

Various classes of waves are forced in the fluid outer core. Tides and wobbles of the rotation axis drive inertial waves, whereas seismic forcing leads to the propagation of sound waves. However, this chapter focuses mainly on waves that are internally driven. Disturbances initiated in some location within the core propagate as waves until some new equilibrium is found. For example, acoustic waves are instrumental in re-equilibrating the pressure field; they are so fast compared to other waves that they are usually filtered out in models of core dynamics, where it is assumed that pressure information is transmitted instantaneously. More generally, competition between the different possible classes of waves is crucial in determining what the most important dynamical constraints on core motions and magnetic fields are.

There is a second motivation to investigate waves propagating inside the core. Determination of their characteristics can lead to new knowledge concerning the hidden magnetic field and the density profile in the core interior. Recently, the average strength of the magnetic field deep inside the core was estimated from the indirect observation of torsional waves recurring every 6 years or so. In Chapter 5.05, Jackson and Finlay discuss other wave-like features that are apparent in successive images of the radial magnetic field at the core surface over the past 400 years. These disturbances, which remain unexplained, are conspicuous near the equator and drift westward.

Finally, it is usual to separately investigate magnetic induction in the core and in the mantle or, similarly, fluid motions in the core and mechanical core–mantle interactions. However, these phenomena are fundamentally coupled together. Complete models of waves inside the core that are currently in development should include mechanisms of coupling with the mantle. The study of these models expounds the limitations of previous models, which were restricted to either the core or the mantle.

8.09.2   Competing Constraints from Rotation and Magnetic Fields

8.09.2.1   Small Disturbances from a Quiescent State

Comprehensive overviews of waves in the presence of rotation and a magnetic field can be found in Gubbins and Roberts (1987) and Finlay (2008).

8.09.2.1.1   Alfvén waves

Waves arise in a liquid metal permeated by a magnetic field because the Lorentz force tends to oppose the curvature of magnetic field lines. In order to introduce the discussion of these so-called Alfvén waves, we study the case of a uniform, steady magnetic field $\mathbf{B}_0$ (see also Finlay (2007) for a deeper physical insight into the mechanism of Alfvén waves). The reader is referred to Chapter 8.03 by Roberts where basic magnetohydrodynamic theory, including the derivation of the induction equation from Ohm's law and Maxwell equations, is presented.

The fluid is assumed to be inviscid and perfectly conducting and to have uniform density ρ. The two coupled momentum and induction equations are linearized to obtain

$$\rho \frac{\partial \mathbf{u}}{\partial t} = -\nabla P + \frac{1}{\mu_0}(\mathbf{B}_0 \cdot \nabla)\mathbf{B} \qquad [1]$$

$$\frac{\partial \mathbf{B}}{\partial t} = (\mathbf{B}_0 \cdot \nabla)\mathbf{u} \qquad [2]$$

where P is a modified pressure, which includes a magnetic pressure term, and μ_0 is the magnetic permeability. Both the magnetic field $\mathbf{B}$ and the velocity field $\mathbf{u}$ are solenoidal:

$$\nabla \cdot \mathbf{u} = \nabla \cdot \mathbf{B} = 0 \qquad [3]$$

Taking the divergence of [1], we obtain

$$\nabla^2 P = 0 \qquad [4]$$

If there are no sources at infinity, $P = 0$.

At this point, it is convenient to introduce the quantities $\mathbf{V}_0 = \mathbf{B}_0/\sqrt{\rho\mu_0}$ and $\mathbf{V} = \mathbf{B}/\sqrt{\rho\mu_0}$, which have the dimensions of a velocity. The set of equations [1] and [2] can then be transformed into a wave equation for $\mathbf{V}$,

$$\frac{\partial^2 \mathbf{V}}{\partial t^2} = (\mathbf{V}_0 \cdot \nabla)^2 \mathbf{V} \qquad [5]$$

and an analogous equation for $\mathbf{u}$ instead of $\mathbf{V}$. It means that fluid or magnetic disturbances transverse to $\mathbf{B}_0$ are propagated in the form of waves. Equations [1] and [2] are both satisfied by solutions of the form

$$\mathbf{u} = \mathbf{f}(\mathbf{x} \pm \mathbf{V}_0 t) \qquad [6]$$

$$\mathbf{V} = \pm\mathbf{f}(\mathbf{x} \pm \mathbf{V}_0 t) \qquad [7]$$

where $\mathbf{f}$ is an arbitrary function and $\mathbf{x}$ is the position vector. The solutions are specified by the initial values of $\mathbf{u}$ and $\mathbf{V}$. Seeking plane wave solutions $\mathbf{u} \propto \exp[i(\mathbf{k}\cdot\mathbf{x} - \omega t)]$, where $\mathbf{k}$ denotes the wave vector and ω the frequency, we obtain the dispersion relation

$$\omega = \pm(\mathbf{V}_0 \cdot \mathbf{k}) = \pm k(\mathbf{V}_0 \cdot \mathbf{1}_k) \qquad [8]$$

where $\mathbf{1}_k$ is the unit vector along the direction of $\mathbf{k}$. Thus, the phase speed $c = (\omega/k)$ of the Alfvén waves in the direction of $\mathbf{k}$ is directly given by the Alfvén velocity $\mathbf{V}_0$. The group velocity

$\partial\omega/\partial\mathbf{k}$ (i.e., $(\partial\omega/\partial k_x, \partial\omega/\partial k_y, \partial\omega/\partial k_z)$ in Cartesian coordinates (x, y, z)) is defined as the velocity of energy propagation. It is $\mathbf{V}_0$ for all directions of $\mathbf{k}$.

Expressions [6] and [7] show clearly that there is equipartition of energy: the energy density of Alfvén waves is equally distributed among its kinetic $\rho u^2/2$ and magnetic $B^2/2\mu_0 = \rho V^2/2$ components.

Finally, Alfvén waves act as the means of eliminating discontinuities in the tangential components of the magnetic field at the surface of an electrically conducting fluid when there is a magnetic field transverse to the boundary. This effect was first documented by Stewartson (1957) in the case of a perfectly conducting and inviscid fluid half-space abutting a solid and insulating domain. In the presence of kinematic viscosity ν and magnetic diffusivity η, dissipative effects are restricted to a thin boundary layer. The nature of this 'Hartmann' boundary layer depends on the value of the magnetic Prandtl number, $p_m = \nu/\eta \ll 1$ (Busse et al., 2007, pp 137–138). In the limit $p_m \ll 1$, which is appropriate for liquid metals, only the velocity field is modified through the boundary layer and to erase the magnetic field discountinuities, Alfvén waves are emitted (Roberts and Scott, 1965). Thus, the dissipation-free interior problem (outside the boundary layer) is required to satisfy not only normal boundary conditions but also tangential ones.

8.09.2.1.2   Inertial waves

Inertial waves are caused solely by rotation. The reader is referred to Chapter 8.07 by Tilgner for a complete discussion of inertial oscillations in rotating spheres and spherical shells. Once again, an inviscid, incompressible, and infinitely extended fluid is considered. Chapter 8.07 details how the momentum equation, expressed in a frame of reference rotating with the angular frequency $\mathbf{\Omega}$,

$$\rho \frac{\partial \mathbf{u}}{\partial t} + 2\rho(\mathbf{\Omega} \times \mathbf{u}) = -\nabla p \qquad [9]$$

can be transformed into the equation

$$\frac{\partial^2}{\partial t^2}\nabla^2\mathbf{u} + 4(\mathbf{\Omega}\cdot\nabla)^2\mathbf{u} = 0 \qquad [10]$$

Searching for plane wave solutions, which are suitable for the short-wavelength limit, we obtain the dispersion equation

$$\omega = \pm\frac{2\mathbf{k}\cdot\mathbf{\Omega}}{k} \qquad [11]$$

The frequency ω is independent of the wavelength and the typical period is of the order of the rotation period of the fluid. In contrast to Alfvén waves, inertial waves are strongly dispersive. From eqn [11], the group velocity can be calculated:

$$\mathbf{c}_g = \pm 2\frac{\mathbf{1}_k \times (\mathbf{\Omega} \times \mathbf{1}_k)}{k} \qquad [12]$$

Thus, the energy transport is at right angles to the planes of the constant phase. It can also be shown that the result $|\omega| \leq 2\Omega$, obtained here for plane waves in an infinite domain, also holds for inertial oscillations in a contained rotating fluid (Greenspan, 1965).

In the limit $\omega = 0$, which corresponds to $(\mathbf{1}_k \cdot \mathbf{\Omega}) = 0$, there is geostrophic balance between the Coriolis and pressure terms.

From eqn [10], we learn that there is an excitation of inertial waves when the Proudman–Taylor theorem

$$(\mathbf{\Omega}\cdot\nabla)\mathbf{u} = 0 \qquad [13]$$

is violated. In other words, inertial waves will ring until the velocity field is modified in such a way that it satisfies eqn [13]. This state is reached quickly as exemplified by the formation of a 'Taylor' column, named after the famous experiments reported by Taylor (1923), above a disk co-rotating with an infinite body of fluid. In an insightful thought experiment (Davidson, 2001, p. 165; Greenspan, 1968, pp. 192–200), one can imagine a disk of radius r_0 being made to move slowly along the axis of rotation and perpendicular to its own surface at the initial time $t=0$. The axisymmetric fluid velocity is sought as a function of time. The initial value problem can be solved analytically and the solution is given in Greenspan (1968). On each side of the disk and within the axial cylinder C circumscribing the disk, there is a region of increasing size where the fluid particles move with the disk. Outside the cylinder C, the fluid is at rest in the rotating frame of reference. The height of the region moving with the disk increases with time as $\Omega r_0 t$. This finding is consistent with an interpretation in terms of inertial waves as the front velocity corresponds to the group velocity of plane inertial waves, with the wave vector perpendicular to the rotation axis, and a wavenumber of r_0^{-1}. In Earth's core of radius r_c, we expect that Taylor columns of radius l reach the core–mantle boundary (CMB) in both hemispheres after a time of the order $(r_c/l)\Omega^{-1}$.

In a container, the boundaries have significant influence on large-wavelength inertial waves. In the case of the full sphere, implicit solutions for the oscillations and their frequencies were calculated long ago by Bryan (1889). Zhang et al. (2001) relied on the work of Kudlick (1966) to derive explicit solutions for the inertial waves. They paid special attention to the slowest waves, which are almost invariant in the direction parallel to the rotation axis as expected from eqn [11]. They found that the angular frequency of these quasi-geostrophic inertial waves (QGIW) is

$$\omega_R \sim \frac{2\Omega}{m+2}\left(\sqrt{1 + \frac{m(m+2)}{N(2N+2m+1)}} - 1\right) \qquad [14]$$

where the flow evolves as $\exp[i(m\phi - \omega t)]$ and N increases with the complexity in the s-direction (s, ϕ, z are cylindrical polar coordinates). The sign of ω_R in eqn [14] tells us that the phase of the QGIW waves propagates in the prograde (eastward) direction. For a given m, their frequency decreases as the length scale in the s-direction shortens.

QGIW waves have the character of Rossby waves (hence, the subscript R given earlier), which were first described in the meteorological context. Their mechanism can be visualized by considering a fluid column directed parallel to the rotation axis (**Figure 1**). In the case of the full sphere, the column acquires vorticity when displaced radially inward because it is stretched (Busse, 2002). Conversely, it loses vorticity when shifted outward. Later, eqn [14] is compared with the dispersion equation for Rossby waves after the quasi-geostrophic approximation is introduced (see **Section 8.09.2.2.2**).

When an inner sphere is present, solutions of the inviscid inertial wave equation present singular surfaces (Rieutord et al., 2001). Then, it is necessary to reinstate viscosity to obtain continuous solutions.

8.09.2.1.3 Compressibility effects

The density of the core increases by about 20% from the CMB down to the inner core boundary (ICB). This observation motivates our discussion of compressibility effects. Taking into account compressibility slightly modifies the equations for inertial waves and geostrophic motions. Here, the consequences are illustrated by using a general anelastic framework (Anufriev et al., 2005; Braginsky and Roberts, 1995).

Adiabatic stratification. The anelastic continuity equation is

$$\nabla\cdot(\rho_a\mathbf{u}) = 0 \qquad [15]$$

where ρ_a is the density in an adiabatically stratified reference state. It approximates the conservation of mass equation and governs processes having characteristic time scales, large with respect to acoustic periods, thus eliminating seismic waves from the problem.

In a compressible fluid, pressure variations p cause density variations ρ':
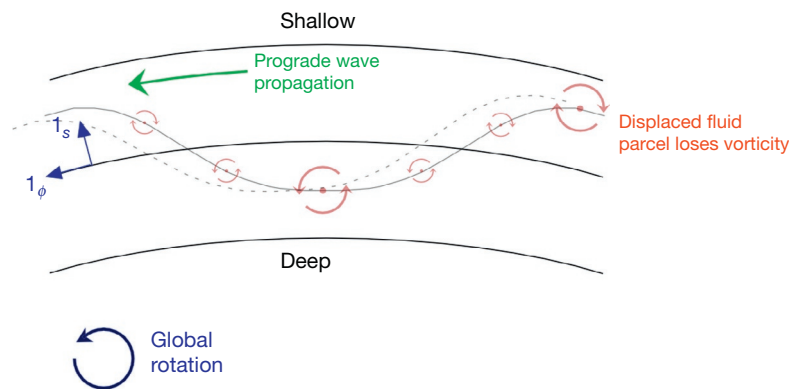
Figure 1 Mechanism of hydrodynamic Rossby waves visualized in the equatorial plane of a spherical shell with large aspect ratio. Vorticity acquired in response to the displacement relative to the rotation axis of axial fluid filaments. Prograde (eastward) propagation of the perturbation.

$$\rho' = p\left(\frac{\partial \rho_a}{\partial p}\right)_{S, \xi} \qquad [16]$$

where the entropy S and the composition ξ are kept constant assuming the perturbation to be adiabatic. In the spherically symmetric adiabatic reference state, the pressure and gravitational terms are in hydrostatic balance

$$\frac{dp_a}{dr} = -g\rho_a \qquad [17]$$

where $\mathbf{g} = -g\mathbf{1}_r$ is the gravitational acceleration, and eqn [16] transforms into

$$\rho' = -\frac{p}{g\rho_a}\frac{d\rho_a}{dr} \qquad [18]$$

The momentum equation

$$\rho_a\frac{\partial \mathbf{u}}{\partial t} + 2\rho_a(\mathbf{\Omega} \times \mathbf{u}) = -\nabla p + \rho'\mathbf{g} \qquad [19]$$

can then be written as:

$$\rho_a\frac{\partial \mathbf{u}}{\partial t} + 2\rho_a(\mathbf{\Omega} \times \mathbf{u}) = -\rho_a\nabla\frac{p}{\rho_a} \qquad [20]$$

Assuming a steady state and dropping the first term on the left-hand side, a modified Proudman–Taylor constraint is obtained from eqns [15] and [20]. It holds here only for the components of the velocity field $\mathbf{u}_\perp$ perpendicular to the rotation axis,

$$(\mathbf{\Omega}\cdot\nabla)\mathbf{u}_\perp = 0 \qquad [21]$$

as a direct consequence of

$$(\mathbf{\Omega}\cdot\nabla)\left(\frac{p}{\rho_a}\right) = 0 \qquad [22]$$

From [15], we find that the velocity component u_z parallel to the rotation axis depends on z when $u_s \neq 0$:

$$\frac{\partial}{\partial z}(\rho_a u_z) = -u_s\frac{\partial}{\partial s}\rho_a \qquad [23]$$

These results hold in the framework of the more complete theory of Braginsky and Roberts (1995), provided that pressure p is replaced by an effective pressure $p + \rho_a U'$ in eqn [22], although their theory accounts for the perturbation U' in the gravitational potential, which has been neglected here.

Gravity waves. Gravity waves arise in the presence of both thermal and compositional density gradients (e.g., Gubbins and Roberts, 1987) when the reference state (p_0, ρ_0) is not exactly adiabatic. The hydrostatic balance [17] holds now for p_0 and ρ_0:

$$\frac{dp_0}{dr} = -g\rho_0(r) \qquad [24]$$

We consider radial displacement η_r of a fluid parcel initially at rest, which occurs fast enough to be adiabatic, that is, with negligible heat transfer. The density difference between the displaced parcel and its new environment is:

$$\delta\rho = \eta_r\left[\left(\frac{\partial \rho}{\partial r}\right)_{S, \xi} - \frac{d\rho_0}{dr}\right] \qquad [25]$$

and the fluid parcel is subjected to the force $-\delta\rho g\mathbf{1}_r$. Newton's second law gives

$$\rho_0\frac{\partial^2 \eta_r}{\partial t^2} = -\delta\rho g \qquad [26]$$

The two equations [25] and [26] define the buoyancy (or Brunt–Väisälä) frequency N:

$$N^2 = \frac{g}{\rho_0}\left[\left(\frac{\partial \rho}{\partial r}\right)_{S, \xi} - \frac{d\rho_0}{dr}\right] \qquad [27]$$

N is imaginary when the buoyancy exerts a restoring force on the fluid parcel and the stratification is stable. Note that this description does not yet account for the horizontal displacement of matter caused by the rising fluid parcel.

Next, displacement is separated into its radial and horizontal parts, $\delta\mathbf{r} = \eta_r\mathbf{1}_r + \boldsymbol{\eta}_H$. Velocity can be expressed as the rate of change of the displacement of the fluid parcel, that is, $\mathbf{u} = \partial\delta\mathbf{r}/\partial t$. Linearizing about the reference state, the equation of motion may be written as

$$\rho_0\frac{\partial \mathbf{u}}{\partial t} = -\nabla p' + \rho'\mathbf{g} \qquad [28]$$

Expanding the perturbation variables (pressure p' and displacement $\boldsymbol{\eta}$) as $\exp[i(\mathbf{k}\cdot\mathbf{r} - \omega t)]$, where n is the wavenumber in the radial direction and k is the wavenumber in the horizontal direction, the radial and horizontal parts of eqn [28] are

$$-\rho_0\omega^2\eta_r = -inp' - \rho'g \qquad [29]$$

$$-\rho_0\omega^2\boldsymbol{\eta}_H = -i\mathbf{k}_Hp' \qquad [30]$$

Integrating the equation of continuity [15] with respect to time and neglecting $\eta_r d\rho_0/dr$ compared to $n\eta_r\rho_0$ gives

$$n\eta_r + \mathbf{k}_H\cdot\boldsymbol{\eta}_H = 0 \qquad [31]$$

Substituting between these yields

$$\rho_0\omega^2\left(1 + \frac{n^2}{k^2}\right)\eta_r = \rho'g \qquad [32]$$

From [25] and [27], we also have

$$\rho'g = \rho_0N^2\eta_r \qquad [33]$$

Combining [32] and [33], the dispersion relation for gravity waves is obtained:

$$\omega^2 = \frac{k^2}{k^2 + n^2}N^2 \qquad [34]$$

Note that the frequency is always less than N. If the horizontal wavelength of a disturbance is much shorter than its vertical wavelength (i.e., $k^2 \gg n^2$), then the frequency of the gravity waves is simply $\omega = N$, independent of the wavelength.

8.09.2.2 Constraint Imposed by Rapid Rotation

The importance of rotation in a non-magnetized fluid is characterized by the Rossby number Ro, which is defined as the ratio of the advective and Coriolis terms (Vallis, 2006):

$$Ro(l) = \frac{U}{\Omega l} \qquad [35]$$

where l is a characteristic length scale in directions at right angles to the axis of rotation and U, a typical velocity. For large-scale dynamics in Earth's core, the term $\mathbf{V}\cdot\nabla\mathbf{V}$ arising from the Lorentz force dominates the advective term $\mathbf{u}\cdot\nabla\mathbf{u}$ and the ratio λ of the magnetic and Coriolis terms is, thus, the appropriate number to characterize the relative importance of rotation:

$$\lambda(l) = \frac{V_{\mathrm{A}}}{l\Omega} = \frac{\mathcal{B}}{\sqrt{\mu_0\rho}\,l\Omega} \qquad [36]$$

where $\mathcal{B}$ is a typical magnetic field strength inside the core and V_{A}, the associated Alfvén wave speed $V_{\mathrm{A}} = \mathcal{B}/\sqrt{\mu_0\rho}$. We refer to λ, where λ is a shorthand for $\lambda(r_{\mathrm{c}})(=V_{\mathrm{A}}/r_{\mathrm{c}}\Omega)$ and we have taken $l = r_{\mathrm{c}}$ as the Lehnert number for the application to Earth's core. This acknowledges an early theoretical study of magnetohydrodynamic waves in the presence of rotation that identified λ as the key parameter (Lehnert, 1954). The Lehnert number is also the ratio of the periods of inertial and Alfvén waves (Jault, 2008). Other names are used too. In this volume, Paul Roberts introduces λ as the magnetic Rossby number (Ro_{m}, according to his notation) while Chris Jones, following Christensen and Aubert (2006), denotes it Lo (for Lorentz number). The Lehnert number can also be thought of in terms of a group velocity. It is the ratio of the speeds at which Alfvén and inertial waves carry information and energy.

For wavenumber $k < \lambda^{-1}$, the rapid propagation of inertial waves brings about the formation of Taylor columns; hence, motions with wavenumber $k < \lambda^{-1}$ can be expected to be almost axially invariant (e.g., Staplehurst et al., 2008). For $k > \lambda^{-1}$, Alfvén waves have a higher frequency than inertial waves and small-scale columnar structures have no time to develop. Thus, the length λr_{c} approximately demarks the scale of the transition between 2D (axially invariant) and 3D dynamics as recently illustrated by Gillet et al. (2011), who documented the change from 2D to 3D dynamics with increasing wavenumber in a spherical shell geometry appropriate to Earth's fluid core (Figure 2).

8.09.2.2.1 Quasi-geostrophic approximations

The quasi-geostrophic framework involves the assumption that the flow is to leading order in geostrophic balance, and that variations in the axial direction are small compared to those in directions at right angles to the rotation axis. It was pioneered in the context of core dynamics by Hide (1966) and formally developed within the context of convection in a rotating annulus by Busse (1970).

We begin with the conservation of momentum in a rotating, electrically conducting, incompressible fluid (see Chapter 8.05, equation [1])

$$\rho\frac{\partial\mathbf{u}}{\partial t} + \rho(\mathbf{u}\cdot\nabla)\mathbf{u} + 2\rho(\mathbf{\Omega}\times\mathbf{u}) = -\nabla p + \mathbf{j}\times\mathbf{B} \qquad [37]$$

Buoyancy and viscous forces have been neglected here, so as to focus attention on the interplay between the Coriolis and Lorentz forces.

We treat Earth's core as a spherical container. We proceed to nondimensionalize, using its radius r_{c} as a typical length scale, $\mathcal{B}$ as a typical magnetic field, $V_{\mathrm{A}} = \mathcal{B}/\sqrt{\mu_0\rho}$ as a typical velocity, ρV_{A}^2 for the pressure scale, and $r_{\mathrm{c}}/V_{\mathrm{A}}$ for the time scale, to obtain
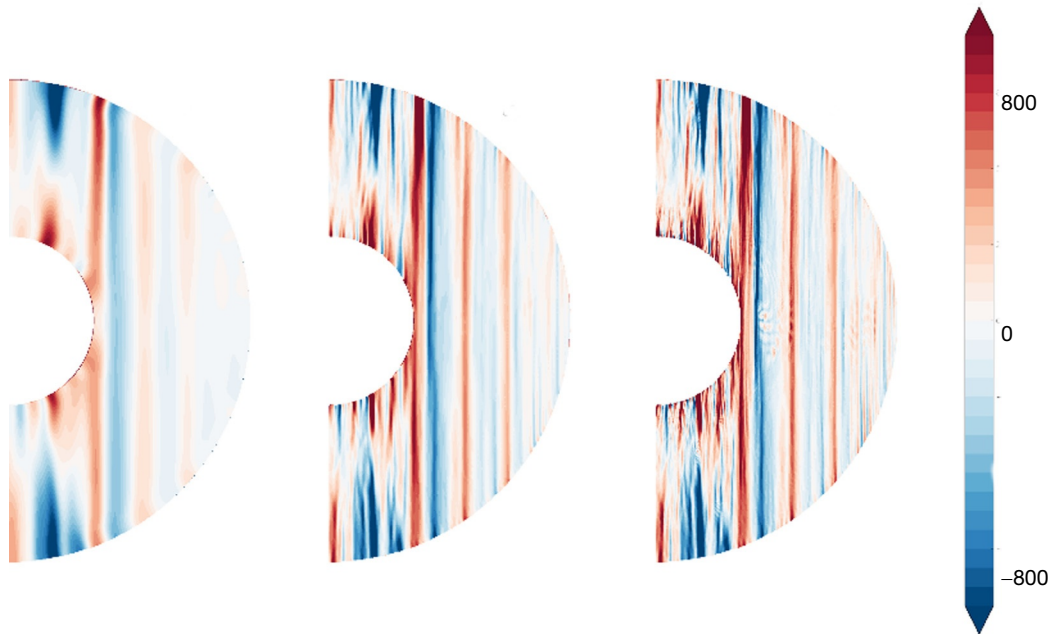
Figure 2 Quasi-geostrophy of velocities with large scales in directions at right angles to the rotation axis. A meridian slice (snapshot) of the azimuthal velocity extracted from a rapidly rotating dynamo model driven by mass anomaly flux at the two boundaries (see, e.g., Aubert et al., 2009) with $p_{\mathrm{m}} = 0.1$ and Ekman number $\nu/\Omega(r_{\mathrm{c}} - r_i)^2 = 10^{-7}$, leading to Rossby number $Ro \sim 6\times10^{-4}$ and Lehnert number $\lambda \sim 10^{-3}$. Less and less small scales are filtered out from left to right, illustrating the progressive loss of quasi-geostrophy as the length scale is decreased. Left and middle: scales respectively smaller than $0.1r_{\mathrm{c}}$ and $0.02r_{\mathrm{c}}$ are filtered out. Right: full solution. Personal communication from N. Schaeffer (see also Chapter 8.06).

$$\frac{\partial \mathbf{u}}{\partial t} + (\mathbf{u}\cdot\nabla)\mathbf{u} + 2\lambda^{-1}(\mathbf{1}_z \times \mathbf{u}) = -\nabla p + \mathbf{j} \times \mathbf{B} \qquad [38]$$

where λ is the Lehnert number $\lambda(r_c)$ taking the length scale $l = r_c$ (see [36]). In cylindrical polar coordinates (s, ϕ, z), the shape of its outer boundary is defined by the heights $z = H_c(s)$ above and $z = -H_c(s)$ below the equatorial plane, where $H_c(s) = \sqrt{r_c^2 - s^2}$.

Two different versions of the quasi-geostrophic framework are described here. To begin with, we follow the classical approach proposed by Busse (1970), developed in order to investigate the onset of thermal convection (which occurs far from the equator) in an internally heated, rapidly rotating fluid sphere. It involves expanding the velocity and pressure fields into power series consisting of increasing powers of α, where α is the slope of the outer boundary

$$\alpha(s) = \frac{dH_c(s)}{ds} = -\frac{s}{H_c} \qquad [39]$$

For example, the velocity field is expanded as

$$\mathbf{u} = \mathbf{u}_0 + \mathbf{u}_1 + \cdots \qquad [40]$$

where $\mathbf{u}_0 \simeq \mathcal{O}(1)$, $\mathbf{u}_1 \sim \mathcal{O}(\alpha)$, etc. This series will converge provided $|\alpha| \ll 1$. Further assuming that $\lambda \ll 1$ (its value is thought to be $\sim 10^{-4}$ in Earth's core), to leading order there is simply geostrophic balance

$$2\lambda^{-1}(\mathbf{1}_z \times \mathbf{u}_0) = -\nabla p_0 \qquad [41]$$

and $\mathbf{u}_0$ obeys the Proudman–Taylor theorem [13]. To leading order, the quasi-geostrophic flow is, therefore, two-dimensional, without variations in the axial direction. The geostrophic solution [41] is completed by the boundary condition $(\mathbf{1}_z\cdot\mathbf{u}_0) = 0$, which is the rigid boundary condition when there is no boundary slope, as is appropriate for this order.

Since the leading order flow is two-dimensional, it can be written in terms of a scalar stream function Ψ,

$$\mathbf{u}_0 = \nabla \times (\Psi \mathbf{1}_z) = \left(\frac{1}{s}\frac{\partial \Psi}{\partial \phi}, -\frac{\partial \Psi}{\partial s}, 0\right) \quad \text{where} \quad \Psi = -\frac{p_0\lambda}{2} \qquad [42]$$

Moving to the next order in the expansion provides a prognostic equation, describing the time evolution of the geostrophic flow $\mathbf{u}_0$,

$$\frac{\partial \mathbf{u}^0}{\partial t} + (\mathbf{u}_0\cdot\nabla)\mathbf{u}_0 + 2\lambda^{-1}(\mathbf{1}_z \times \mathbf{u}_1) = -\nabla p_1 + \mathbf{j} \times \mathbf{B} \qquad [43]$$

If there was no magnetic force on the right-hand side of [43], we would find that $\partial p_1/\partial z = 0$ and that the velocity components parallel to the equatorial plane are z-invariant at the first order in α. The reasoning is less straightforward in the presence of a magnetic force (or, for that matter, of a buoyancy term with a nonzero z-component). An equation for the evolution of the axial component of vorticity v

$$v = \mathbf{1}_z\cdot(\nabla \times \mathbf{u}_0) = -\nabla_\perp^2 \Psi$$

where

$$\nabla_\perp^2 = \frac{1}{s}\frac{\partial}{\partial s}\left(s\frac{\partial}{\partial s}\right) + \frac{1}{s^2}\frac{\partial^2}{\partial \phi^2} \qquad [44]$$

can, nevertheless, be obtained by taking the z component of the curl of eqn [43]

$$\frac{D}{vt}v - 2\lambda^{-1}\frac{\partial u_{1z}}{\partial z} = \mathbf{1}_z\cdot\nabla \times (\mathbf{j} \times \mathbf{B}) \qquad [45]$$

where $D/Dt = \partial/\partial t + (\mathbf{u}_0\cdot\nabla)$, and we have made use of the incompressibility condition $\nabla\cdot\mathbf{u}_1 = 0$, which holds at this order since we have already assumed $\nabla\cdot\mathbf{u}_0 = 0$ at the leading order. Next comes a crucial step: averaging over the axial direction $\mathbf{1}_z$. The term Dv/Dt is unchanged, and the term arising from the Coriolis force is readily simplified as follows:

$$-\frac{\lambda^{-1}}{H_c}\int_{-H_c}^{H_c}\frac{\partial u_{1z}}{\partial z}dz = -2\lambda^{-1}\beta(s)u_{0s} \quad \text{where} \quad \beta(s) = \frac{\alpha}{H_c} \qquad [46]$$

Here, the no-penetration boundary condition at the top and bottom sloping boundaries has been used:

$$\mathbf{u}\cdot(\mathbf{1}_z \mp \nabla H_c) = u_{1z} \mp \alpha u_{0s} = 0 \quad \text{at} \ z = \pm H_c \qquad [47]$$

Notice that $\mathbf{u}_1$ has been eliminated without specifying its value in the interior.

The resulting axially averaged equation for the evolution of the axial vorticity is

$$-\frac{D}{Dt}v + 2\lambda^{-1}\beta u_s = -\frac{1}{2H_c}\int_{-H_c}^{H_c}\mathbf{1}_z\cdot\nabla \times (\mathbf{j} \times \mathbf{B})dz \qquad [48]$$

Although this small α version of the quasi-geostrophic model has proved very successful in studies of thermal convection in a spherical geometry, even in supercritical situations (Gillet and Jones, 2006), using it to study the core dynamics underlying geomagnetic secular variation is problematic on a number of counts. First, it is obviously not correct in the equatorial region where $\alpha \to \infty$. Second, although the z-invariance of QG flows makes the QG apparatus appropriate for continuing into the core interior the surface flows (u_θ, u_ϕ) inverted from geomagnetic data (Pais and Jault, 2008, see Chapter 8.04), the flow equation [42] does not obey the no-penetration condition $\mathbf{u}_0\cdot\mathbf{1}_r = 0$ and so it has to be modified to match the surface flow. Simply adding a z-component u_{1z} such that eqn [47] is obeyed for $\mathbf{u}_0$ is not satisfactory because, then, the total flow is not divergence free. For these reasons, an alternative version of the QG model, which is more accurate where the boundary slope is large, has been sought (Schaeffer and Cardin, 2005). This alternative approach is presented next, following the treatment by Becker and Salmon (1997).

The derivation consists in assuming a priori that $\mathbf{u}_\perp$, the velocity perpendicular to the rotation axis, is z-independent. Requiring $\nabla\cdot\mathbf{u} = 0$, we deduce that u_z varies linearly with z because

$$\frac{\partial u_z}{\partial z} = -\nabla_\perp\cdot\mathbf{u} \qquad [49]$$

which is z-independent. From the no-penetration condition

$$u_z = \pm\mathbf{u}_\perp\cdot\nabla H_c \quad \text{at} \ z = \pm H_c \qquad [50]$$

(see eqn [47]) we obtain u_z in the interior

$$u_z = \frac{z}{H_c}(\mathbf{u}_\perp\cdot\nabla H_c) \qquad [51]$$

and [49] can be transformed into

$$\nabla \cdot (H_c \mathbf{u}_\perp) = 0 \qquad [52]$$

The z-integrated equatorial velocity $H_c \mathbf{u}_\perp$ can thus be written as a function of a stream function χ and

$$\mathbf{u} = \frac{1}{H_c} \nabla \times (\chi(s,\phi)\mathbf{1}_z) - \frac{z}{H_c^3} \frac{\partial \chi}{\partial \phi} \mathbf{1}_z \qquad [53]$$

The axial vorticity becomes

$$v = -\frac{1}{H_c} \nabla_\perp^2 \chi - \frac{s}{H_c^3} \frac{\partial \chi}{\partial s} \qquad [54]$$

Equation [48] thus remains valid, but with new expressions for u_s and v.

8.09.2.2.2 Wave motion in a quasi-geostrophic system

In the absence of the magnetic term on the right-hand side and with β constant, eqn [48] is simply the equation for Rossby waves mentioned in Section 8.09.2.1.2. It is usually derived in the (Cartesian) annulus geometry, in which case the term $\beta \partial \psi / s \partial \phi$ is transformed into $\beta \partial \psi / \partial x$. Rossby waves arise naturally in the perturbation approach outlined earlier. At the leading order, the flow is geostrophic and z-invariant. At the next order, ageostrophy (i.e., deviation from geostrophy) arises because the height of fluid columns parallel to the rotation axis depends on the cylindrical radius. This weak ageostrophy is responsible for the slow prograde wave propagation.

Here, we explore what happens to such Rossby waves in the presence of a simple magnetic field. Following Acheson (1978), we consider a uniform imposed field aligned along the prograde direction in a geometry consisting of a rotating fluid layer between the top and bottom boundaries of a constant slope, that is, unbounded in the cylindrical radial direction. With this setup, neglecting curvature, we are able to work in a local Cartesian coordinate system, with z in the axial direction, x the prograde direction, and y directed toward the rotation axis (i.e., in the direction of increasing fluid depth). Thus, the imposed magnetic field is

$$\mathbf{B}_0 = B_0 \mathbf{1}_x \qquad [55]$$

We make the additional hypothesis that a small magnetic field perturbation will also be axially invariant (as is reasonable when neglecting magnetic diffusion), so it can be represented as the curl of a scalar magnetic potential $A(x,y)$

$$\mathbf{B}(x,y) = \nabla \times (A(x,y)\mathbf{1}_z) \qquad [56]$$

Since the fluid layer is unbounded in the y direction, the layer depth H is used to nondimensionalize length and it is this that appears in the Lehnert number labeled $\lambda_H = B_0 / \sqrt{\rho \mu_0} \Omega H$. The linearized equations governing the evolution of small perturbations of the axial vorticity and magnetic field are then

$$\frac{\partial}{\partial t} \nabla_\perp^2 \Psi + 2\lambda_H^{-1} \beta \frac{\partial \Psi}{\partial x} = -\frac{\partial}{\partial x} \nabla_\perp^2 A \qquad [57]$$

$$\frac{\partial A}{\partial t} = -\frac{\partial \Psi}{\partial x} \qquad [58]$$

Here, $\nabla_\perp^2 = \partial^2/\partial x^2 + \partial^2/\partial y^2$.

Using trial solutions (Ψ, A) proportional to $\exp[i(k_x x + k_y y - \omega t)]$, and substituting from eqn [58] into eqn [57] to eliminate A, the following quadratic dispersion relation is obtained:

$$\omega^2 + 2\lambda_H^{-1} \frac{\beta k_x}{k^2} \omega - k_x^2 = 0 \quad \text{with } k^2 = k_x^2 + k_y^2 \qquad [59]$$

which permits two solutions

$$\omega = \lambda_H^{-1} \frac{\beta k_x}{k^2} \left(-1 \pm \sqrt{1 + \frac{\lambda_H^2 k^4}{\beta^2}} \right) \qquad [60]$$

When the Lehnert number λ_H is small, the two roots separate, taking the distinct forms

$$\omega_R = -2\lambda_H^{-1} \frac{\beta k_x}{k_2} \quad \text{and} \quad \omega_{MR} = \frac{\lambda_H k_x k^2}{2\beta} \qquad [61]$$

The physical nature of these waves becomes clear on moving back to dimensional units

$$\omega_R = -2\Omega \frac{\beta k_x}{k^2} \quad \text{and} \quad \omega_{MR} = \frac{B_0^2}{\rho_0 \mu_0 2\Omega \beta} k_x k^2 \qquad [62]$$

Recall that we have defined our β parameter without including the rotation rate Ω. The solution ω_R corresponds to Rossby waves, and the contribution of the magnetic energy to the total energy of this wave is only $O(\lambda^2)$. The other solution, $\omega_{MR,}$ depends fundamentally on both the magnetic field and rotation for its existence. It is known as a magnetic Rossby wave, and it propagates in the opposite direction to the hydrodynamic Rossby wave and with a much lower frequency. It is, therefore, sometimes referred to as the 'slow' wave and is characterized by magnetostrophic balance, inertia being negligible because of the low frequency. In magnetic Rossby waves, time changes in the velocity field occur via time changes in the magnetic field. Hide (1966) argued that in the rotation-dominated, hydromagnetic regime of Earth's core, such waves may be relevant for explaining some aspects of geomagnetic secular variation including the westward motion of magnetic field features. Such features with azimuthal wavenumber $m = 5$ in the equatorial region of the core surface were later discovered by Finlay and Jackson (2003). The section "Magnetic-Coriolis waves" in Finlay et al. (2010) provides a recent review of magnetic Rossby waves including the quest for experimental evidence.

We note here in passing that propagation of hydrodynamic Rossby waves provides a mechanism for establishing a magnetostrophic balance between the Coriolis and magnetic terms in eqn [48].

8.09.2.2.3 Axially averaged equations

In this section, we assume that magnetic surface terms (which appear when we are taking the axial average of the terms arising from the Lorentz force) may be neglected because the magnetic field at the core surface is smaller than that in the core interior. Defining an axial averaging operator

$$\langle X \rangle = \frac{1}{2H_c} \int_{-H_c}^{H_c} X \, dz \qquad [63]$$

and then expanding the terms on the right-hand side of eqn [48] due to the Lorentz force, following Canet et al. (2009) we find

$$-\frac{D}{Dt}v + 2\lambda^{-1}\beta(s)u_s = \left(\frac{1}{s}\frac{\partial}{\partial s}\frac{\partial}{\partial \phi} + \frac{1}{s^2}\frac{\partial}{\partial \phi}\right)\left(\langle B_s^2 \rangle - \langle B_\phi^2 \rangle\right)$$
$$-\left(\frac{3}{s}\frac{\partial}{\partial s} - \frac{1}{s^2}\frac{\partial^2}{\partial \phi^2} + \frac{\partial^2}{\partial s^2}\right)\langle B_s B_\phi \rangle \qquad [64]$$

Note that the ϕ component of the Navier–Stokes equation, averaged over both the axial and azimuthal directions, directly gives the time evolution of the zonal component of the flow:

$$\frac{\partial \zeta}{\partial t} = \frac{1}{2\pi s^3 H_c}\frac{\partial}{\partial s}\left(s^2 H_c\left[\oint \langle B_s B_\phi \rangle d\phi\right]\right) \quad \text{where} \quad \zeta(s) = u_G(s)/s \quad [65]$$

This is particularly useful when the geometry of the system is restricted to the region ($s \geq r_i$) outside the cylindrical surface tangent to the solid inner core of radius r_i (as in Canet et al. (2009)). Indeed, the vorticity equation [64] leaves the zonal component of the flow undetermined in a multiply connected domain such as a cylindrical annulus (Plaut and Busse, 2002). The subscript G in [65] indicates that axially invariant zonal velocities $u_\phi(s)\mathbf{1}_\phi$ form the geostrophic part of the velocity field in spherical geometry. On the one hand, they satisfy both eqns [41] and [47]. On the other hand, the ageostrophic perturbation u_z is zero if and only if $u_s = 0$ (see eqn [47] or eqn [51]). Geostrophic velocities do not contribute to the Coriolis term in the vorticity equation [64]. Given later (see eqn [81]) are the surface terms modifying [65], which have been neglected at this stage. Equation [65] prescribes the evolution of $u_G(s)$ and is key to our later discussion of torsional waves (Section 8.09.3.2).

Canet et al. (2009) have also shown that, provided one neglects magnetic diffusion, the induction equation can similarly be axially averaged in order to obtain relations for the evolution of the quadratic quantities $\langle B_s^2 \rangle$, $\langle B_\phi^2 \rangle$, and $\langle B_s B_\phi \rangle$ that appear in eqn [64]. With the definition [53] for the quasi-geostrophic velocity field, their expression is modified slightly and the following relations obtained:

$$\frac{\partial}{\partial t}\langle B_s^2 \rangle = -H_c(\mathbf{u}\cdot\nabla_\perp)\left(\frac{1}{H_c}\langle B_s^2 \rangle\right) + 2\langle B_s^2 \rangle\frac{\partial u_s}{\partial s} + 2\frac{\langle B_s B_\phi \rangle}{s}\frac{\partial u_s}{\partial \phi}$$

$$\frac{\partial}{\partial t}\langle B_\phi^2 \rangle = -\frac{1}{H_c}(\mathbf{u}\cdot\nabla_\perp)\left(H_c\langle B_\phi^2 \rangle\right) + 2s\langle B_s B_\phi \rangle\frac{\partial}{\partial s}\left(\frac{u_\phi}{s}\right) - 2\frac{\partial u_s}{\partial s}\langle B_\phi^2 \rangle$$

$$\frac{\partial}{\partial t}\langle B_s B_\phi \rangle = -(\mathbf{u}\cdot\nabla_\perp)\langle B_s B_\phi \rangle + s\langle B_s^2 \rangle\frac{\partial}{\partial s}\left(\frac{u_\phi}{s}\right) + \frac{1}{s}\langle B_\phi^2 \rangle\frac{\partial u_s}{\partial \phi}$$

$$[66]$$

The coupled equations [64]–[66] govern the time evolution of $\chi, \zeta, \langle B_s^2 \rangle, \langle B_\phi^2 \rangle$, and $\langle B_s B_\phi \rangle$ in the regions $[0, r_c]$ or $[r_i, r_c]$. They have to be supplemented by boundary conditions at the two circles delimiting the domain. The no-penetration condition gives $\partial \chi/\partial \phi = 0$. The boundary condition for ζ at $s = r_c$ is derived from the fact that the magnetic field that leaves the disk is continuous to a potential field. We give this condition in Section 8.09.3.3, where torsional waves are discussed. Additional restrictions on χ, which are also required to ensure continuity of the magnetic field at the boundary with the insulator, have yet to be worked out.

Considerable simplifications of the quasi-geostrophic model [64]–[66] result if one makes the additional hypothesis, introduced earlier in the course of our exposition of Rossby waves, that the magnetic field is also axially invariant:

$$\mathbf{B}(s,\phi) = \nabla \times (A(s,\phi)\mathbf{1}_z) \qquad [67]$$

Substitution into the Navier–Stokes and magnetic induction equations yields the simple coupled system

$$\frac{D}{Dt}\nabla_\perp^2 \Psi + \frac{2\lambda^{-1}\beta(s)}{s}\frac{\partial \Psi}{\partial \phi} = -(\mathbf{B}\cdot\nabla)\nabla_\perp^2 A \qquad [68]$$

and

$$\frac{\partial A}{\partial t} = -(\mathbf{u}_0\cdot\nabla)A + \frac{1}{S}\nabla_\perp^2 A \qquad [69]$$

Here, $S = r_c V_A/\eta$ is known as the Lundquist number, and it describes the ratio between the magnetic diffusion time scale and the Alfvén wave time scale. The assumption of an axial invariant magnetic field is certainly very restrictive. However, it has the advantage of allowing magnetic diffusion to be considered within the QG formalism (in the directions perpendicular to the rotation axis), and the resulting equations are more easily solvable both analytically and numerically, while retaining the essential interplay between the magnetic and velocity fields (see, e.g., Tobias et al., 2007).

8.09.2.2.4   Magnetic diffusion layer at the top and bottom boundaries

The main body of the core has been treated as an inviscid and perfectly conducting fluid in order to derive the coupled vorticity and magnetic equations. Furthermore, the quasi-geostrophic velocity field has been defined in such a way that it obeys the no-penetration condition at the top and bottom of the geostrophic cylinders $z = \pm H_c$. The velocity parallel to the boundary, however, is nonzero (see, e.g., eqn [53]). This situation must be corrected by a viscous (Ekman) boundary layer, with a thickness of $(\nu/\Omega)^{1/2}$. The question thus arises whether there is also a boundary layer for the magnetic field through which its tangential discontinuities can be accommodated.

Such discontinuities are to be expected because the magnetic field components $\mathbf{B}_\parallel$ and B_n, parallel and transverse to the boundary, respectively, are related. Provided the domain outside the fluid cavity is treated as an electrical insulator, the magnetic field derives from a unique potential scalar V, $\mathbf{B} = -\nabla V$, with V obeying the Laplace's equation $\nabla^2 V = 0$. Potential theory then tells us that the specification of the normal component $B_n = -(\nabla V)_n$ at the boundary determines V and, thus, $\mathbf{B}$ uniquely in the outer insulating domain.

In the absence of rotation, any discontinuities of the tangential magnetic field in the boundary layer at the fluid–solid interface are eliminated through the emission of Alfvén waves as long as $\mathbf{B}\cdot\mathbf{n} \neq 0$ (see Section 8.09.2.1.1). Rapid rotation, however, rigidifies the fluid in the axial direction and hinders the propagation of Alfvén waves normal to the boundary (Backus, 1968, Appendix II). The discontinuities are, accommodated, instead, through a magnetic diffusive boundary layer. Its thickness can be calculated as in a solid conductor. This description holds as long as rapid rotation prevents significant shear from developing in the axial direction.

8.09.2.2.5   Quasi-geostrophic MHD turbulence

Diamond et al. (2007) have discussed β-plane MHD turbulence (eqns [68] and [69]) to clarify the turbulent mixing of momentum and magnetic field in the solar tachocline, where

the dynamics is two-dimensional as the result of a strong stable stratification. They note that quasi-geostrophic turbulence in a spherical shell is characterized by the coexistence of Rossby waves and Alfvén waves at different length scales.

The frequency (eqn [62], left) of Rossby waves to the frequency [8] of Alfvén waves can, indeed, be compared. The wavenumber $k_0 = (\beta\Omega/V_A)^{1/2}$ corresponds to the boundary between Alfvénic and Rossby dominated ranges. At large length scales ($k < k_0$), the turbulence is that of a sea of Rossby waves. At small length scales, with wavenumbers above k_0, it can be anticipated that Alfvén waves redistribute equally the energy between the kinetic and magnetic components.

At the beginning of this section, it was noted that a second wavenumber $k_1 = \lambda^{-1} = \Omega/V_A$ can be formed from the frequencies of Alfvén and 3D inertial waves. Quasi-geostrophic approximations hold for $k < k_1$, with $k_0 \leq k_1$ (see also Chapter 8.06).

8.09.3 Torsional Waves

Torsional waves consist of geostrophic motions. In a spherical shell, geostrophic flows depend only on the distance s to the rotation axis and their velocity can be expressed as $s\zeta(s)\mathbf{1}_\phi$. Any differential rotation ($\mathrm{d}\zeta/\mathrm{d}s \neq 0$) between rigid geostrophic cylinders shears the magnetic field and propagates similarly to Alfvén waves in the direction of either increasing or decreasing s (Figure 3). Estimating the propagation speed of torsional waves gives an estimate of the squared magnetic field strength averaged over the geostrophic cylinders. Torsional waves arise in response to violations of Taylor's condition, which is now introduced.

8.09.3.1 Taylor's Condition

Taylor (1963) considered an incompressible fluid contained in an axisymmetric, rigid, envelope Σ. He investigated the conditions under which there exists a velocity $\mathbf{u}$ in a magnetostrophic balance:
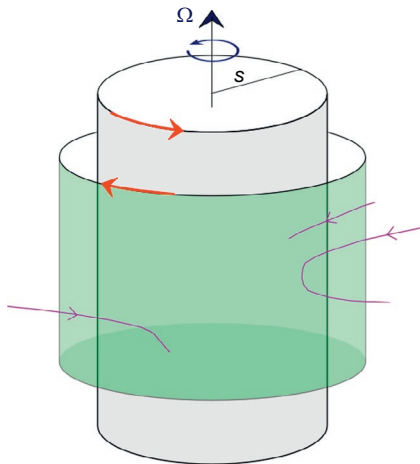
Figure 3 Torsional wave mechanism. All the magnetic field scales contribute to the restoring Lorentz force acting on geostrophic cylinders that is responsible for torsional wave propagation.

$$2\rho(\mathbf{\Omega} \times \mathbf{u}) + \nabla p = \mathbf{F},$$

$$\text{with } \mathbf{F} = \mathbf{j} \times \mathbf{B} + \rho'\mathbf{g}, \quad \nabla \cdot \mathbf{u} = 0, \quad \text{and} \qquad [70]$$

$$\mathbf{u} \cdot \mathbf{n}|_\Sigma = 0 \qquad [71]$$

where $\mathbf{n}$ is the unit outward normal to Σ. The necessary and sufficient condition for the existence of a solution is that the inhomogeneity $\mathbf{F}$ is orthogonal to each solution of the adjoint homogeneous problem (where the inner product is defined by the energy norm as in Busse (1970)). The homogeneous part of the equation reduces to a geostrophic balance

$$2\rho(\mathbf{\Omega} \times \mathbf{u}) + \nabla p = 0 \qquad [72]$$

The solution consists of geostrophic motions $\mathbf{u}_G = 1/2\Omega(\mathbf{1}_z \times \nabla p)$. In order to derive the equations for the adjoint homogeneous problem, eqn [72] is multiplied scalarly by the adjoint field $\mathbf{v}$:

$$\forall \mathbf{u}, \quad \int \mathbf{v} \cdot (2\rho(\mathbf{\Omega} \times \mathbf{u}) + \nabla p)\mathrm{d}V = 0$$

$$\forall \mathbf{u}, \quad \int -\mathbf{u} \cdot (2\rho(\mathbf{\Omega} \times \mathbf{v}))\mathrm{d}V + \int \mathbf{u} \cdot \nabla\pi\,\mathrm{d}V + \int_\Sigma p(\mathbf{v} \cdot \mathbf{n})\mathrm{d}\Sigma = 0$$

$$[73]$$

where eqn [71] has been used to introduce the new term involving π. The adjoint homogeneous problem is simply

$$-2\rho(\mathbf{\Omega} \times \mathbf{v}) + \nabla\pi = 0 \qquad [74]$$

together with the no-penetration condition ($\mathbf{v} \cdot \mathbf{n} = 0$) at the boundary.

As a result, geostrophic motions $\mathbf{u}_G$ are also solutions of the adjoint problem and the following solvability condition has to be satisfied for arbitrary geostrophic motions:

$$\forall \mathbf{u}_G, \quad \iiint \mathbf{u}_G \cdot \mathbf{F}\,\mathrm{d}V = 0 \qquad [75]$$

So far, the derivation remains valid in non-axisymmetric cavities and we use later, in Section 8.09.4.2, the constraint,

$$\forall \mathbf{u}_G, \quad \iiint \mathbf{u}_G \cdot (\mathbf{j} \times \mathbf{B})\mathrm{d}V = 0 \qquad [76]$$

derived from the additional assumption $\mathbf{u}_G \cdot \mathbf{g} = 0$, which holds when either the buoyancy is neglected or the boundary is axisymmetric. In the latter case, the geostrophic cylinders are circular, $\mathbf{u}_G = s\zeta(s)\mathbf{1}_\phi$, and eqn [76] can be transformed into the constraint originally derived by Taylor (1963),

$$\forall s, \quad \iint_{\Sigma(s)} (\mathbf{j} \times \mathbf{B})_\phi s\,\mathrm{d}\phi\,\mathrm{d}z = 0 \qquad [77]$$

where $\Sigma(s)$ denotes the cylindrical surface $s = $ constant. Paul Roberts obtains this constraint from a slightly different but fundamentally equivalent approach in the section "MHD geodynamo theory" in Chapter 8.03.

Smylie et al. (1984) generalized the condition [76] to compressible fluids by adopting the subseismic approximation, which is closely related to the anelastic approximation (Rieutord and Dintrans, 2002). It can, indeed, be readily demonstrated that eqn [76] also holds for an anelastic fluid, where

$$2\rho_a(\mathbf{\Omega} \times \mathbf{u}) + \rho_a\nabla\frac{p}{\rho_a} = \mathbf{F}, \quad \text{with } \nabla \cdot \rho_a\mathbf{u} = 0, \quad \mathbf{u} \cdot \mathbf{n}|_\Sigma = 0 \quad [78]$$

provided its solid envelope is axisymmetric. Then, geostrophic motions are again of the form $\mathbf{u}_G = s\zeta(s)\mathbf{1}_\phi$ (see the Proudman–Taylor condition [21] derived in the compressible case) and are solutions of the adjoint homogeneous problem.

When eqn [76] does not hold, it is necessary to reinstate the geostrophic acceleration term in the momentum equation.

8.09.3.2   The Canonical One-Dimensional Torsional Wave Equation

Roberts and Aurnou (2012) have introduced the qualifier 'canonical' in order to refer to the equation for torsional waves in the spherical geometry and in its simplest form, without complications arising from non-axisymmetric terms or from the nonvanishing mantle conductivity. It is remarkable that the equations for torsional waves reduce to a second-order differential equation for the geostrophic angular velocity $\zeta(s,t)$, where the magnetic field enters only through a function of s:

$$\{V_s^2\}(s) = \frac{1}{\rho\mu_0\hat{\Sigma}_g(s)}\int_{\Sigma_g(s)} B_s^2\, s\, \mathrm{d}z\, \mathrm{d}\phi \qquad [79]$$

where $\hat{\Sigma}_g(s)$ denotes the area of the geostrophic cylinder $\Sigma_g(s)$ of radius s, and density ρ is uniform. The integral in eqn [79] involves all the length scales of the magnetic field.

Braginsky (1970) presented torsional waves as a possible mechanism for the changes in length of day, initially with periods of about 60 years. He gave the original derivation of their equation, which can also be found in Roberts and Soward (1972) and Jault (2003). The equation for the time evolution of the geostrophic velocity is part of the axially averaged equations presented in Section 8.09.2.2.3, but there eqn [65] is only approximate. In fact, it is possible to calculate rigorously the boundary terms, which are neglected in eqn [65]. As already mentioned, there is geostrophic acceleration when eqn [77] does not hold, so

$$4\pi\rho H_c \frac{\partial u_G(s)}{\partial t} = \int_{-H_c}^{H}\oint (\mathbf{j}\times\mathbf{B})_\phi\, \mathrm{d}\phi\, \mathrm{d}z = \frac{1}{\mu_0}\int_{-H_c}^{H_c}\oint \nabla\cdot(s\mathbf{B}_M B_\phi)\, \mathrm{d}\phi\, \mathrm{d}z \qquad [80]$$

where $\mathbf{B}_M$ is the field in the meridional plane $(\mathbf{1}_s, \mathbf{1}_z)$ and H_c, hereafter, is dimensional. Before linearizing, we can separate the last term on the right into volume and surface parts:

$$4\pi\rho\mu_0 H_c \frac{\partial u_G}{\partial t} = \frac{1}{s^2}\frac{\partial}{\partial s}\left(s^2\int_{-H_c}^{H_c}\oint B_s B_\phi\, \mathrm{d}\phi\, \mathrm{d}z\right)$$
$$+ \frac{r_c}{H_c}\left(\oint B_r B_\phi\, \mathrm{d}\phi(H_c) + \oint B_r B_\phi\, \mathrm{d}\phi(-H_c)\right) \qquad [81]$$

The linearization consists in treating the time-dependent quantities as small perturbations of a static basic state. Substituting eqn [66] for $\partial\left(\int_{-H_c}^{H_c} B_s B_\phi\, \mathrm{d}z\right)/\partial t$ (with $\mathbf{u}_0 = s\zeta(s)\mathbf{1}_\phi$) into the time derivative of eqn [81], we obtain

$$\frac{\partial^2\zeta}{\partial t^2} = \frac{1}{s^3 H_c}\frac{\partial}{\partial s}\left(s^3 H_c\{V_s^2\}\frac{\partial^2\zeta}{\partial s}\right) + \text{surface terms} \qquad [82]$$

All surface terms depend on the radial magnetic field at the CMB. Assuming that the conductivity of the mantle is weak enough, it is possible to separate these terms into two groups.

One introduces a nonlocal coupling between the geostrophic cylinders, regardless of the lower mantle conductivity, when the magnetic field is not symmetrical about the rotation axis. It has been shown, using a realistic model of the magnetic field in the core interior, that this does not affect the propagation of torsional waves much (Jault and Légaut, 2005; Roberts and King, 2013). The other surface terms involve the conductivity of the lower mantle. They cause electromagnetic coupling between the core and the mantle (Dumberry and Mound, 2008).

It is straightforward to generalize eqn [82] to the case of an anelastic fluid core:

$$\frac{\partial^2\zeta}{\partial t^2} = \frac{1}{\mathcal{P}(s)}\frac{\partial}{\partial s}\left(\mathcal{P}(s)\overline{\{V_s^2\}}\frac{\partial\zeta}{\partial s}\right) + \text{surface terms} \qquad [83]$$

with

$$\mathcal{P}(s) = s^3 H_c\bar{\rho},\ \bar{\rho}(s) = \frac{1}{H_c}\int_0^{H_c}\rho(s,z)\, \mathrm{d}z \quad \text{and} \quad \overline{\{V_s^2\}}$$
$$= \frac{1}{\bar{\rho}\mu_0\hat{\Sigma}_g(s)}\int_{\Sigma_g(s)} B_s^2 s\, \mathrm{d}z\, \mathrm{d}\phi \qquad [84]$$

8.09.3.3   Boundary Conditions for the One-Dimensional Torsional Wave Equation

As the propagation of torsional waves is not directly affected by the Coriolis force, the arguments presented earlier (Section 8.09.2.1.1) concerning the appropriate boundary conditions, in the absence of rotation, for the coupled momentum and induction equations in the limit of vanishing viscosity and magnetic diffusivity are fully relevant here. Schaeffer et al. (2012) have recently discussed, in this particular context, why the value of the magnetic Prandtl number p_m is crucial, notwithstanding both v and η are vanishingly small, for the wave reflection at $s=r_c$.

In the relevant limit $p_m \ll 1$, the thin boundary layer involves only the velocity field, and the magnetic field is left unchanged throughout the layer. The boundary conditions for the diffusionless outer problem include a continuity condition for all magnetic field components. If it is assumed that the mantle is electrically insulating, the magnetic field involved in the torsional wave propagation has to match with a potential field at $s=r_c$. At the boundary, the radial electrical currents vanish and the zonal magnetic field is also zero:

$$\mu_0 j_r = \mu_0 j_s = \mathbf{1}_s\cdot(\nabla\times\mathbf{B}) = 0, \quad \oint B_\phi\, \mathrm{d}\phi = 0, \quad \text{at } s = r_c \quad [85]$$

We now seek to transform [85] into a boundary condition on ζ. We develop $\partial j_s/\partial t = 0$ using the frozen flux induction equation for the magnetic field parallel to the boundary (at $s=r_c$)

$$\frac{\partial B_\phi}{\partial t} = -\zeta\frac{\partial B_\phi}{\partial\phi} + sB_s\frac{\partial\zeta}{\partial s}, \quad \frac{\partial B_z}{\partial t} = -\zeta\frac{\partial B_z}{\partial\phi} \qquad [86]$$

Thus, we have

$$\forall\phi, \quad \mu_0\frac{\partial}{\partial t}j_s = -s\frac{\partial\zeta}{\partial s}\frac{\partial B_s}{\partial z} = r_c\frac{\partial\zeta}{\partial s}\left(\frac{\partial B_s}{\partial\theta}\right),$$
$$\frac{\partial\zeta}{\partial s}\Big|_{s=r_c}\left(\frac{\partial B_r}{\partial\theta}\right)_{r=r_c,\,\theta=\pi/2} = 0 \qquad [87]$$

Taking the time derivative of the second equation [85], we similarly obtain

$$\frac{\partial \zeta}{\partial s}\bigg|_{s=r_c} \oint B_r(r_c, \pi/2, \phi)\, \mathrm{d}\phi = 0 \qquad [88]$$

The two equations [87] and [88] yield $\partial \zeta/\partial s = 0$ at $s = r_c$, which, in turn, suffices to ensure that the two constraints [85] remain satisfied.

Interestingly, this result has been obtained without any considerations regarding the vanishing height of the geostrophic cylinders as $s \to r_c$. In this respect, Schaeffer et al. (2012) studied numerically how a geostrophic pulse actually reflects in a spherical cavity at $s = r_c$. For $p_m = 1$, they found that there is no reflection at all as on a vertical wall. For $p_m < 1$, however, the reflection coefficients R on the inside of a spherical boundary and on a wall parallel to the rotation axis differ. In both cases, R increases as $p_m \to 0$ (from $R = 0$ at $p_m = 1$), but the spherical boundary is much less reflective (see their Figure 3). For $p_m = 10^{-3}$, $R \sim 0.8$ in the spherical case.

8.09.3.4 Inference of the Strength of the Magnetic Field in Earth's Core Interior

Several authors have interpreted the zonal and equatorially symmetric part of core surface flows inverted from geomagnetic data as the signature of normal modes of the fluid core consisting of standing torsional waves referred to as torsional oscillations (Bloxham et al., 2002; Zatman and Bloxham, 1997). In these studies, the input flow $u_\phi(\theta,t) = u_\phi(\pi - \theta, t)$ either for the period 1900–90 or for ~1950–2000. To begin with, a few normal modes are fitted to $u_\phi(\theta,t)$. Second, a model of the squared propagation velocity $\{V_s^2\}(s)$ (see definition [79]) is inverted from the periods and the geometry of the normal modes. The period of the modes decreases with the spatial complexity and is about 80 years (i.e., comparable to the 60-year period initially considered by Braginsky) for the mode with the simplest geometry.

The expression of the geostrophic angular velocity $\zeta(s)$ as a combination of normal modes for the time span 1840–1990 (covered by the *gufm1* magnetic field model of Jackson et al. (2000)) has been used by Buffett et al. (2009) to calculate the Green's function, which describes the response of the fluid core to an impulsive excitation. They have obtained source functions, eigenmodes and eigenfrequencies, from their flow model $u_\phi(\theta,t)$.

Estimates of $\{V_s^2\}(s)$ can be translated into magnetic field strengths, which are typically 0.2–0.3 mT (for a basic period of 80 years), about the same as the r.m.s. (root mean square) radial magnetic field at the CMB (0.3 mT). This result is in conflict with the distribution of the magnetic field in numerical simulations of the geodynamo (e.g., Aubert et al., 2009). Such dynamo models display magnetic fields in the core interior with an r.m.s. field amplitude about ten times stronger than the dipole field at the core surface, and imply an intensity of several mT within Earth's core.

Note that there are, of course, other magnetic field changes with both shorter and longer time scales (e.g., Jackson, 2003). Magnetic variations (and length-of-day fluctuations) in the period range 60–80 years have perhaps received most attention because they were the first to be well characterized; this was because of the length and resolution of the time series then available. Roberts et al. (2007) present a more positive viewpoint concerning the 60–80-year signal.

In contrast, Gillet et al. (2010) have recently argued that torsional waves propagate much more rapidly than previously thought. They have attributed both the length-of-day (l.o.d.) and magnetic variations recurring every 6 years to torsional waves emitted periodically from the vicinity of the geostrophic cylinder circumscribing the inner core. As a consequence of the increased propagation velocity of torsional waves, Gillet et al. (2010) have revised upward the r.m.s. strength of the magnetic field in the cylindrical radial direction to approximately 3 mT (Figure 4). The geophysical evidence supporting the new value for the velocity $\{V_s^2\}^{1/2}$ is now outlined.

At frequencies less than 1/5 cycles per year, fluctuations of the atmospheric winds and oceanic currents seem insufficient to cause the observed length-of-day variations (Gross et al., 2004). In fact, a persistent 6-year oscillation in the l.o.d. signal appears more clearly after subtracting contributions to the l.o.d. from the motions in the outer fluid envelope of Earth (Abarca del Rio et al., 2000). This 6-year oscillation was first interpreted as geodetic evidence of gravitational coupling between the laterally heterogeneous mantle and the inner core (Mound and Buffett, 2006). There is also direct evidence for a magnetic signal with the same frequency. Silva et al. (2012) have identified a 6-year periodic signal from the CHAOS3 (1997–2010) and CM4 (1960–2002) geomagnetic field models. These results are consistent with the findings of Gillet et al. (2010), who recovered a 6-year period in the spectrum (over 1925–90) of the l.o.d. variations predicted from their core flow models, which are in phase with the actual l.o.d. changes observed over the same time span.

Provided that the distribution of magnetic energy in the core interior is approximately isotropic, 3 mT r.m.s. strength of the magnetic field in the cylindrical radial direction corresponds to 5 mT typical intensity of the total field (since $3\sqrt{3} \sim 5$). From this value, which agrees approximately with an independent estimate inferred from anomalous dissipation in nutations (Buffett, 2010), it is calculated that the magnetic
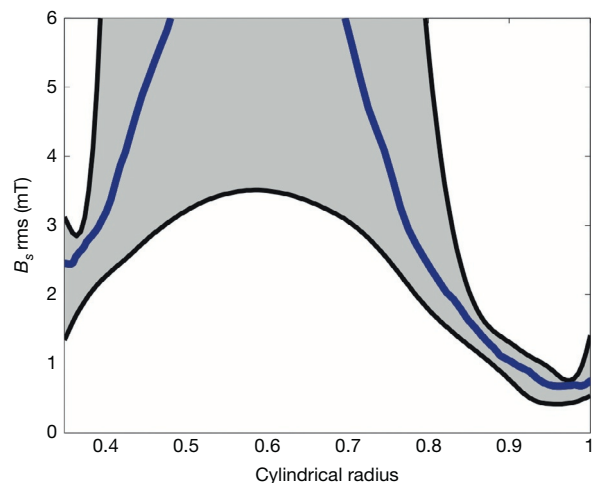
Figure 4 The r.m.s. value of the cylindrical radial magnetic field $B_s(s)$ in the core interior averaged over geostrophic cylinders, as a function of distance to the rotation axis. Reproduced from Gillet, N., Jault, D., Canet, E., Fournier, A., 2010. Fast torsional waves and strong magnetic field within the Earth's core. Nature 465, 74–77.

energy density in the core is about 20 J m^{-3}. The kinetic energy density of large-scale motions, which is about 2×10^{-3} J m^{-3} for a typical velocity 5×10^{-4} m s^{-1}, is thus tiny compared to the total magnetic energy density. This statement is in agreement with the discussion in Section 8.09.2.2.5. At the wavenumber k_0, magnetic and velocity fields have comparable energies. However, for $k < k_0$, $\mathbf{u} \cdot \nabla \mathbf{u} \ll \mathbf{V} \cdot \nabla \mathbf{V}$, and the magnetic energy dominates the kinetic one. According to this picture of Earth's core MHD, transfer of energy between different scales occurs via the magnetic term for $k < k_0$.

Finally, identifying the time evolution of the geostrophic angular velocity $\zeta(s)$ with the propagation of torsional waves constrains the geostrophic shear at $s = r_c$ beneath the equator of the core. As a result, there can be a contradiction between the physical constraint $\partial \zeta / \partial s = 0$ at $s = r_c$ (for the case of an insulating mantle) and the core surface flows obtained in kinematic inversions of magnetic data. The difficulty can be traced to the type of the step-by-step approach currently used to model core dynamics. The solution is to invert for the parameters of the torsional waves directly from geomagnetic data and belongs to the realm of data assimilation (Fournier et al., 2010).

8.09.3.5   Calculation of Core Angular Momentum Changes

Presented here is the calculation of the variations in mantle angular momentum, and thus in l.o.d., which compensate the variations in core angular momentum caused by time changes of the geostrophic velocity (Jackson et al., 1993; Jault et al., 1988). Due account is taken of the increase in core density with depth, which does not modify the expression of the geostrophic velocity as $s\zeta(s,t)$ (see eqn [21]) provided that the boundary is symmetrical about the rotation axis.

Mathews et al. (1991) calculated the equatorial moment of inertia A_c of Earth's core from the density profile of the PREM model. They also estimated the dynamical ellipticity e of Earth's core. From these two values, the axial moment of inertia $C_c = A_c/(1-e)$ of the core is found to be about 9.14×10^{36} kg m^2. The moment of inertia C_m of the solid Earth (crust and mantle) is about 7.12×10^{37} kg m^2, whereas the moment of inertia of the solid inner core is comparatively very small, 5.87×10^{34} kg m^2. The inner core is ignored here on the basis of its small angular momentum. In order to calculate the angular momentum carried by geostrophic motions, it is convenient to have an analytical expression for the density profile $\rho(r)$ in the core. To this end, the expression of Labrosse et al. (2001), also used in Chapter 8.02, is adopted:

$$\rho(r) = \rho_c \exp\left(-\frac{r^2}{L_\rho^2}\right) \quad [89]$$

where $\rho_c = 1.25 \times 10^4$ kg m^{-3} is the density at the center and $L_\rho = 7.4 \times 10^6$ m is the length scale for the compression. It is based on the logarithmic equation of state of Poirier and Tarantola (1998) and on the development to the third order of the radius of the gravity profile. Equation [89] is inserted in the expression for the core moment of inertia about the rotation axis:

$$C_c = \iiint r^4 \rho(r) \sin^3\theta \, dr \, d\theta \, d\phi \quad [90]$$

with the above values for ρ_c and L_ρ and $C_c = 9.15 \times 10^{36}$ kg m^2 is found to be in good agreement with the value quoted earlier.

The geostrophic velocity $u_G(s)$ is calculated, from magnetic observations, in the mantle rest frame. Thus, the core angular momentum, in an inertial frame is

$$\sigma_c = C_c \Omega(t) + \sigma_c'$$
$$\sigma_c' = \iiint \rho(r) s^2 u_G(s,t) \, ds \, d\phi \, dz \quad [91]$$

We insert eqn [89] into [91] and obtain

$$\sigma_c' = 2\pi\sqrt{\pi} L_\rho \rho_c \int_0^{r_c} s^2 u_G(s) \, \text{erf}\left(\frac{H_c}{L_\rho}\right) \exp\left(-\frac{s^2}{L_\rho^2}\right) ds \quad [92]$$

In the incompressible limit ($L_\rho \to \infty$), we have

$$\sigma_c' = 4\pi\rho_c \int_0^{r_c} s^2 u_G(s) H_c \, ds = 4\pi\rho_c r_c^4 \int_0^1 x^2 \sqrt{1-x^2} u_G(x) \, dx \quad [93]$$

(with $x = H_c/r_c$) since

$$L_\rho \, \text{erf}\left(\frac{H_c}{L_\rho}\right) \exp\left(-\frac{s^2}{L_\rho^2}\right) = \frac{2H_c}{\sqrt{\pi}} \left(1 - \frac{H_c^2 + 3s^2}{3L_\rho^2} + O\left(\frac{r_c}{L_\rho}\right)^4\right) \quad [94]$$

At the core surface, the geostrophic flow is part of the toroidal flow and can be written as

$$u_G = \nabla \times (Tr) = \sum_{l=0}^{\infty} t_{2l+1}^0 \nabla \times (P_{2l+1}^0(\cos\theta)r), \quad u_G = -\frac{\partial T}{\partial \theta} 1_\phi \quad [95]$$

where T is the toroidal scalar and $P_l^0(x)$ is the Legendre polynomial of degree l, and the odd parity stems from the symmetry with respect to the equatorial plane. Thus, not only at the surface (where $\partial P_l^0(\cos\theta/\partial\theta) = P_l^1(\cos\theta)$) but also in the entire volume, as a consequence of geostrophy,

$$u_G = -\sum_{l=0}^{\infty} t_{2l+1}^0 P_{2l+1}^1(x) \quad [96]$$

where P_l^1 is the associated Legendre function of degree l and order 1. The functions $(P_{2l+1}^1)l$ form the basis of orthogonal functions over $[0,1]$ for the L^2 inner product.

We then insert

$$x^2\sqrt{1-x^2} = -\frac{1}{5}P_1^1(x) - \frac{2}{15}P_3^1(x) \quad [97]$$

together with eqn [96], in [93] and use

$$\int_0^1 P_l^1(x^2) \, dx = \frac{l(l+1)}{2l+1} \quad [98]$$

to obtain

$$\sigma_c' = \frac{8\pi}{15}\rho_c r_c^4 \left(t_1^0 + \frac{12}{7}t_3^0\right) = \frac{C_c}{r_c}\left(t_1^0 + \frac{12}{7}t_3^0\right) \quad [99]$$

where C_c is also expressed in the incompressible limit ($L_\rho \to \infty$) in order to preserve the consistency of the derivation.

The same steps can be followed to calculate σ_c' at the next orders in $(r_c/L)^2$ analytically. Successive approximations are constructed for σ_c' (as given by eqn [92] and expressions extending eqn [94]) for increasing powers of $(r_c/L_\rho)^2$, from the incompressible result $\sigma_c' = C_c(t_1^0 + 1.714 t_3^0)/r_c$ to $\sigma_c' = C_c(t_1^0 + 1.786 t_3^0 + 0.0910 t_5^0)/r_c$ at the first order and $\sigma_c' = C_c(t_1^0 + 1.777 t_3^0 + 0.0789 t_5^0 + 0.002 t_7^0)/r_c$ at the second order. The direct numerical calculation (substituting expression [96] for u_G in eqn [92]) gives $\sigma_c' = C_c(t_1^0 + 1.776 t_3^0 + 0.0796 t_5^0 + 0.002 t_7^0 + 4.10^{-5} t_9^0 + \cdots)/r_c$. From the rapid convergence of the numerical factors multiplying the coefficients t_{2l+1}^0, we conclude that the incompressible approximation is adequate for the calculation of core angular momentum changes.

Changes in core angular momentum are compensated by changes in mantle angular momentum to preserve the total angular momentum of Earth:

$$(C_m + C_c)\frac{d\Omega}{dt} \sim -\frac{C_c}{r_c}\frac{d}{dt}\left(t_1^0 + 1.776 t_3^0 + 0.080 t_5^0 + 0.002 t_7^0\right) \quad [100]$$

The changes in length of day δT (measured in milliseconds) are thus related to the changes in the flow coefficients (measured in kilometers per year) through

$$\delta T \sim 1.232\left(\delta t_1^0 + 1.776\,\delta t_3^0 + 0.080\,\delta t_5^0 + 0.002\,\delta t_7^0\right) \quad [101]$$

We recommend using the numerical factor 1.232 instead of 1.138 adopted in most previous investigations of core angular momentum changes. The difference stems from a discrepancy between estimates of C_c.

8.09.4 Mechanical Core–Mantle Interactions

The CMB is not perfectly spherical (see the discussion of the CMB in Chapter 1.23). The dynamical ellipticity of the fluid core is one of the parameters entering nutation models, which give an ellipticity value in excess of the hydrostatic value. The extra flattening of the CMB is estimated to be about 400 m (Mathews et al., 2002). This result can constrain 3D geodynamic models of mantle density and seismic wave speeds (Simmons et al., 2010), which in turn give models of the large-scale CMB topography. According to these models, negative topography occurs beneath subducting slabs (in the circum-Pacific region) and positive topography at the base of upwelling regions (Lassak et al., 2010; Soldati et al., 2012; Yoshida, 2008). However, these deviations from a gravity equipotential surface are reduced in the presence of a layer of very low viscosity in the lowermost mantle. An additional source of CMB topography is isostatic compensation of lateral thickness variations in a narrow chemically distinct layer above the CMB. Thus, the amplitude of the CMB models varies with the inclusion of several geodynamic features, which may or may not be present in the actual Earth. To conclude and from a geodynamic perspective, CMB height (valley-to-peak) in the range 1–5 km appears plausible. The most recent seismic models of the CMB topography have amplitudes of ±1.5 km. Both Garcia and Souriau (2000) and Sze and van der Hilst (2003) found that PcP, PKP, and PKKP travel time residuals yield peak-to-peak CMB topography of about 3 km. Then, from a collection of PKiKP-PcP travel times, Koper et al. (2003) argued that the peak-to-peak variations of the outer core thickness do not exceed 4 km. Finally, Koelemeijer et al. (2012) have recently investigated the sensitivity of normal modes to the CMB and its vicinity. They find that the peak-to-peak amplitude of CMB topography has to be smaller than 5 km.

The ICB also probably deviates from a surface of revolution. Buffett (1996) assumed that the ICB corresponds approximately to an equipotential surface of Earth's gravity field. These surfaces are not perfectly spherical because the heterogeneous density distribution in the lower mantle creates gravity anomalies. From mantle convection models and the corresponding degree 2 order 2 gravity components, the peak to peak variations of the equatorial inner core radius are estimated to be 100–200 m. Inner core thermal convection may also cause topography at the ICB above the gravity equipotential surfaces. Mizzon and Monnereau (2013) and Deguen et al. (2013) have investigated this, taking into account dynamically induced melting and freezing of the ICB. They show a rapid transition (as a function of the ratio between the phase change time scale and the viscous relaxation time scale) from a convection mode dominated by a degree 1 component (the translation mode of Monnereau et al. (2010) and Alboussière et al. (2010)) to chaotic plume convection. The scale of the convection is reflected in the scale of the induced ICB topography. The discussion here is mostly concerned with the CMB.

8.09.4.1 Geostrophic Contours

The properties of the geostrophic flow in a container of arbitrary shape have been investigated by Greenspan (1965, 1968) and Soward and Roberts (2007). Let us define the geostrophic contours as the curves drawn on the container surface and tangent to the geostrophic flow. In a container filled with an incompressible fluid, pairs of geostrophic contours on the upper $z = z_T$ and lower $z = z_B$ boundaries are separated by a constant height $z_T - z_B = 2H_c$. These curves are the upper and lower rims of geostrophic cylinders, which are not circular in the presence of topography on the core–mantle interface.

Taking into account both the noncircularity of geostrophic cylinders and the adiabatic stratification $\rho_a(r)$ (see Section 8.09.2.1.3) would make the discussion significantly more complicated. Then, the height separating geostrophic streamlines belonging to the same geostrophic cylinder varies with the distance to the rotation axis (see eqn [23]) and geostrophic cylinders do not have a constant height. In the following sections, we keep clear of these subtleties and assume that the density ρ is uniform.

Even though the deviations of the inner and outer boundaries of a nearly spherical shell (such as Earth's fluid core) from a surface of revolution with radii $r = r_i$ and $r = r_c$, respectively, have a small height, there are two regions of the fluid volume where there are no closed geostrophic cylinders. First, the outer boundary may be reentrant in terms of s; it may be locally concave at the equator (Fearn and Proctor, 1992) as illustrated in Figure 5. Second, there is a cylindrical volume void of geostrophic surfaces near $s = r_i$ (see Figure 6). The discussion of the possible dynamical role of these two regions in the excitation or the attenuation of the torsional waves awaits
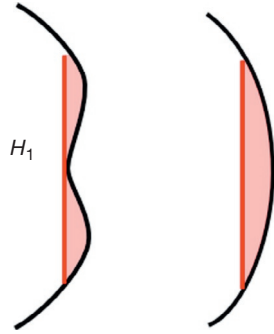
Figure 5 Two meridian slices showing the fluid volume void of geostrophic cylinders (light red) near the outer core equator. The black curve indicates the core–mantle boundary (CMB) and the red curve, a geostrophic cylinder. The figure on the left shows where the CMB is re-entrant. There is no geostrophic contour with height $H_c < H_1$.
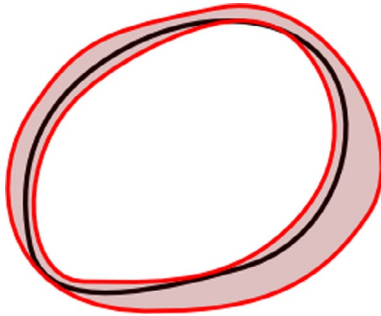
Figure 6 Fluid volume (light red) void of geostrophic cylinders near the inner core equator projected on the equatorial plane. Black curve: projection of the inner core surface. Red curves: geostrophic cylinders closest to the inner core equator. The red inner curve is the projection of the geostrophic cylinder with the largest cross-section above the inner core, and the red outer curve is the projection of the first geostrophic surface circumscribing the inner core.

future studies. We have to leave aside this question. In the following sections, we assume that there are closed geostrophic contours.

The geostrophic velocity and pressure are related by

$$2\rho\Omega\mathbf{u}_G = \mathbf{1}_z \times \nabla p_G \tag{102}$$

The geostrophic pressure is independent of z.

It is convenient to define a set of curvilinear coordinates (q_1, q_2, q_3) such that the geostrophic cylinders correspond to a constant value of one of the coordinates q_1, as illustrated in Figure 7. It is, thus, natural to use a function of H_c as the new curvilinear coordinate q_1 instead of the distance s to the rotation axis, which is appropriate in containers with symmetry about the rotation axis. We define q_3 as a modification of the cylindrical polar coordinate z such that it is constant ($q_3 = \pm H_c$) on pairs of geostrophic contours, where geostrophic cylinders intersect the boundary:

$$q_3 = z + H_c - z_T \tag{103}$$

Then, the unit vector $\mathbf{1}_3$ of the basis remains simply $\mathbf{1}_z$. Following the work of Greenspan (1965) (see also Greenspan, 1968, pp. 43–45), we denote by $\mathbf{n}_T$ and $\mathbf{n}_B$ the unit outward
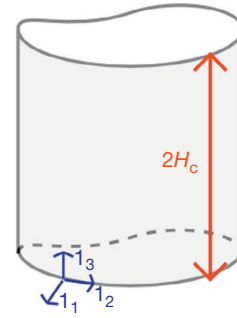
Figure 7 Curvilinear coordinate system (q_1, q_2, q_3). Geostrophic cylinders H_c = constant are coordinate surfaces q_1 = constant. Basis vectors $\mathbf{1}_2$ are tangent to geostrophic contours and $\mathbf{1}_3 = \mathbf{1}_z$.

normals to the outer boundary, respectively, at the top and bottom rims of the geostrophic cylinders. As a consequence of the no-penetration condition $\mathbf{u} \cdot \mathbf{n}_{T,B} = 0$, the vector $\mathbf{n}_T \times \mathbf{n}_B$ is tangent to the geostrophic contours. Thus,

$$\mathbf{1}_2(q_1, q_2) = \frac{\mathbf{n}_T \times \mathbf{n}_B}{|\mathbf{n}_T \times \mathbf{n}_B|} \tag{104}$$

and $\mathbf{1}_1 = \mathbf{1}_2 \times \mathbf{1}_3$ completes the basis. The coordinate q_2 is chosen so that $\mathbf{1}_1$ and $\mathbf{1}_3$ are tangent to the surfaces of the constant q_2. In this coordinate system, the geostrophic velocity can be written as

$$\mathbf{u}_G = u_G(q_1, q_2)\mathbf{1}_2 \tag{105}$$

When the container is symmetrical about the equatorial plane ($z_T = H_c$, $z_B = -H_c$, $q_3 = z$), the geostrophic contours are perpendicular to the rotation axis ($\mathbf{1}_2 \cdot \mathbf{1}_3 = 0$), the vectors ($\mathbf{1}_1$, $\mathbf{1}_2$, $\mathbf{1}_3$) form an orthonormal basis, and the curvilinear coordinates (q_1, q_2, q_3) are orthogonal. We shall adopt this simplification. Then the scale factors h_i fully describe the metric tensor:

$$h_i = \left|\frac{\partial \mathbf{r}}{\partial q_i}\right| \tag{106}$$

where $\mathbf{r}$ is the position vector. Here, the three scale factors $h_1(q_1, q_2)$, $h_2(q_1, q_2)$, and $h_3 = 1$ do not depend on q_3. They replace the set of scale factors ($h_1 = 1$, $h_2 = s$, $h_3 = 1$) for cylindrical polar co-ordinates (s, ϕ, z), used when the container is symmetrical about the rotation axis.

Because $\mathbf{u}_G$ has no component along $\mathbf{1}_1$, the geostrophic pressure depends only on q_1 and eqn [102] reduces to

$$2\rho\Omega h_1 u_G = \frac{\partial p_G}{\partial q_1} \tag{107}$$

Taking the q_2-derivative of eqn [107], we have

$$\frac{\partial}{\partial q_2}(h_1 u_G) = 0 \tag{108}$$

The latter equation can also be obtained from the incompressibility condition $\nabla \cdot \mathbf{u} = 0$, which again gives

$$\frac{\partial}{\partial q_2}(h_1 h_3 u_G) = 0 \tag{109}$$

since the general expression for the divergence in orthogonal curvilinear coordinates is

$$\nabla\cdot\mathbf{u} = \frac{1}{h_1 h_2 h_3}\left(\frac{\partial}{\partial q_1}(h_2 h_3 u_1) + \frac{\partial}{\partial q_2}(h_3 h_1 u_2) + \frac{\partial}{\partial q_3}(h_1 h_2 u_3)\right)$$

[110]

(Morse and Feshbach, 1953, p. 36).

8.09.4.2 Torsional Waves in the Presence of Topography

Sketched out here are possibilities for studying the propagation of torsional waves when the fluid cavity presents deviations from axisymmetry. The derivation of the solvability condition [75] is not contingent on the axisymmetry of the cavity surface (Fearn and Proctor, 1992; Jault, 2003; Soward and Roberts, 2007). It is assumed that the boundary is kept fixed in the rotating frame of reference. For the sake of simplicity, the buoyancy forces are neglected here despite their possible role in this problem. Using eqn [108], eqn [76] can be transformed into

$$\forall q_1, \quad \int_{\Sigma(q_1)} (\mathbf{j}\times\mathbf{B})_2 h_2\, dq_2\, dz = 0$$

[111]

where $\Sigma(q_1)$ is the geostrophic cylinder that is uniquely defined from the constant value taken by the coordinate q_1. Equation [111] generalizes eqn [77]. Fearn and Proctor (1992) remarked, however, that it is misleading to attribute [111] to the need for a torque balance between geostrophic cylinders, which is the definition usually put forward to interpret eqn [77].

When eqn [75] does not hold, as before, it is necessary to restore the geostrophic acceleration term and eqn [80] is generalized to

$$\left(h_1\frac{\partial u_G}{\partial t}\right)(q_1) = \left(s_\rho H_c \oint_{q_1}\frac{h_2}{h_1}\,dq_2\right)^{-1}\int_{\Sigma(q_1)}(\mathbf{j}\times\mathbf{B})_2 h_2\, dq_2\, dq_3$$

[112]

Now the integral on the right-hand side is calculated. It is convenient to write the Lorentz force as

$$\mathbf{j}\times\mathbf{B} = -\frac{1}{2\mu_0}\nabla B^2 + \frac{1}{\mu_0}(\mathbf{B}\cdot\nabla)\mathbf{B}$$

[113]

since the magnetic pressure term $-\nabla p_m$, with $p_m = B^2/(2\mu_0)$, gives a zero contribution to eqn [112]

$$\int_{-H_c}^{H_c}\left(\oint\frac{1}{h_2}\frac{\partial p_m}{\partial q_2}h_2\, dq_2\right)dq_3 = 0$$

[114]

(p_m is single valued).

Using the expression for the operator $(\mathbf{B}\cdot\nabla)$ in generalized orthogonal coordinates (Morse and Feshbach, 1953, p. 33), we have

$$((\mathbf{B}\cdot\nabla)\mathbf{B})_2 = \frac{B_2}{h_2}\frac{\partial B_2}{\partial q_2} + B_3\frac{\partial B_2}{\partial q_3} + \frac{B_1}{h_1}\frac{\partial B_2}{\partial q_1}$$
$$+ \frac{B_1}{h_1 h_2}\left(B_2\frac{\partial h_2}{\partial q_1} - B_1\frac{\partial h_1}{\partial q_2}\right)$$

[115]

because $h_3 = 1$ and $\partial h_2/\partial q_3 = 0$. The first term on the right-hand side gives a zero contribution to the integral of the Lorentz force over a geostrophic cylinder as

$$\oint\frac{B_2}{h_2}\frac{\partial B_2}{\partial q_2}h_2\, dq_2 = 0$$

[116]

Then the expression for the divergence [110] can be used to transform eqn [115] into

$$\int_{\Sigma(q_1)}((\mathbf{B}\cdot\nabla)\mathbf{B})_2 d\Sigma = \int_{\Sigma(q_1)}\left(\frac{\partial}{\partial q_3}(B_2 B_3) + \frac{1}{h_1 h_2^2}\frac{\partial}{\partial q_1}\right.$$
$$\left.(h_2^2 B_1 B_2) + \frac{1}{h_1 h_2}\frac{\partial h_1}{\partial q h_2}(B_2^2 - B_1^2)\right)d\Sigma$$

[117]

where the surface element $d\Sigma$ is $h_2\, dq_2\, dq_3$. The z-integral yields a boundary term that can be written as a function of the magnetic field B_n normal to the boundary. Denoting H_c' the derivative of H_c with respect to q_1, the unit outward normal to the CMB, expressed in the basis $(\mathbf{1}_1, \mathbf{1}_2, \mathbf{1}_3)$, is

$$n = \left(H_c'(q_1)^2 + h_1^2\right)^{-1/2}\left(H_c'(q_1), 0, \pm h_1\right) \quad \text{at } q_3 = \pm H_c$$

[118]

because the equation of the boundary is $q_3 = H_c(q_1)$. After some manipulation, the Lorentz force integrated over $\Sigma(q_1)$ can be written as

$$\int_{\Sigma(q_1)}(\mathbf{j}\times\mathbf{B})_2 h_2\, dq_2\, dq_3 = \frac{1}{\mu_0}\int_{c(q_1)}B_2 B_n\frac{1}{h_1}\left(H_c'(q_1)^2 + h_1^2\right)^{1/2}h_2\, dq_2$$
$$+ \frac{1}{\mu_0}\oint\frac{1}{h_1 h_2}\frac{\partial}{\partial q_1}\left(h_2^1\int_{-H_c}^{H_c}B_1 B_2\, dq_3\right)dq_2$$
$$+ \frac{1}{\mu_0}\int_{\Sigma(q_1)}\frac{1}{h_1 h_2}\frac{\partial h_1}{\partial q_2}(B_2^2 - B_1^2)d\Sigma$$

[119]

where $C(q_1)$ denotes the two rims of the geostrophic cylinder $\Sigma(q_1)$. The last term disappears in spherical geometry, for which $q_1 = s$ and $h_1 = 1$ and the surfaces $q_2 = $ constant have zero curvature C

$$C = -\frac{1}{h_1 h_2}\frac{\partial h_1}{\partial q_2} = 0$$

[120]

Using the identity [108], the frozen flux induction equation gives

$$\frac{\partial B_1}{\partial t} = -\zeta h_1\frac{\partial}{\partial q_2}\left(\frac{B_1}{h_1}\right)$$
$$\frac{\partial B_2}{\partial t} = -\frac{\zeta}{h_1}\frac{\partial}{\partial q_2}(h_1 B_2) + \frac{B_1 h_2}{h_1}\frac{\partial\zeta}{\partial q_1}$$

[121]

where the definition of ζ is generalized here as $\zeta = u_c/h_2$.

Since eqn [111] cannot be directly interpreted in terms of torque balance, a short discussion of the topographic torque acting on the mantle is in order. In the presence of CMB topography, the fluid core locally exerts a pressure force akin to the aerodynamic form drag on the solid mantle. It is now shown that the net torquing effect of the geostrophic pressure on the rotation of the mantle is zero. It is convenient to calculate this pressure torque in the coordinate system (q_1, q_2, q_3) because the geostrophic pressure depends only on q_1. The surface element at the CMB is

$$d\Sigma = \left(H_c'(q_1)^2 + h_1^2\right)^{1/2}h_2\, dq_1\, dq_2$$

[122]

Since the expression [118] for $\mathbf{n}$, the unit outward normal to the boundary has already been derived, the only missing

ingredient to calculate the axial pressure torque $\Gamma_{p,G}$ acting on the CMB is an expression for $s1_s$ in the new coordinate system. Let us define

$$s = g(q_1, q_2) \qquad [123]$$

Then

$$\mathbf{1}_s = \frac{1}{h_1}\frac{\partial g}{\partial q_1}\mathbf{1}_1 + \frac{1}{h_2}\frac{\partial g}{\partial q_2}\mathbf{1}_2 \qquad [124]$$

Finally, it is found that the geostrophic pressure $p_G(q_1)$ exerts no torque on the solid walls

$$\Gamma_{p,G} = \iint_z (s\mathbf{1}_s \times p_G\mathbf{n})\,\mathrm{d}\Sigma$$
$$= \int H_c'(q_1)p_G(q_1)\left(\oint g\frac{\partial g}{\partial q_2}\mathrm{d}q_2\right)\mathrm{d}q_1 = 0 \qquad [125]$$

as the contour integral over q_2 in eqn [125] vanishes.

8.09.4.3   Coupling with the Solid Inner Core

8.09.4.3.1   Time-variable geostrophic contours

If there is differential rotation between the inner and outer boundaries of the fluid core, the two boundaries cannot be simultaneously held fixed in the rotating frame of reference. The no-penetration condition then becomes

$$\begin{aligned} \mathbf{u}\cdot\mathbf{n} &= (\mathbf{\Omega}_i \times \mathbf{r})\cdot\mathbf{n}, \quad \text{at } r = r_i \\ \mathbf{u}\cdot\mathbf{n} &= (\mathbf{\Omega}_o \times \mathbf{r})\cdot\mathbf{n}, \quad \text{at } r = r_c \end{aligned} \qquad [126]$$

where $\mathbf{\Omega}_i$ and $\mathbf{\Omega}_o$ are the angular velocities of the solid core and the mantle, respectively. This differs from eqn [71] only in the presence of topography. If one boundary is symmetric about the axis of rotation, which implies that $\mathbf{1}_\phi\cdot\mathbf{n} = 0$, choosing the rotation of the other as the rotation of the frame of reference makes eqn [126] time invariant. However, it is not possible to choose the rotating frame of reference such that the two conditions [126] are time-invariant if there is topography on both boundaries. Then, the geostrophic contours are time-variable, which yields new inertial acceleration terms in equations written using the system of coordinates (q_1, q_2, q_3) introduced in Section 8.09.4.1.

8.09.4.3.2   Gravitational coupling

There is possibly a gravitational torque between the solid inner core and the mantle because the solid inner core is denser than the fluid outer core and the mantle is laterally heterogeneous (see Chapter 8.08). Buffett (1996) discovered this mechanism and Mound and Buffett (2005) included it in their study of torsional oscillations. They assumed that there is an equilibrium position where the ICB is an equipotential surface of the gravity field. When the inner core rotates through the gravitational and pressure fields, which can be considered fixed in the mantle reference frame, it experiences both a gravitational and a pressure torque. The two torques would exactly cancel out if the solid and fluid cores had the same density because of the hydrostatic equilibrium.

8.09.4.3.3   Electromagnetic coupling

Any differential rotation between the fluid and solid cores results in a strong restoring electromagnetic torque acting between the two bodies. Indeed, the magnetic field in the core interior is stronger than at its surface and both the inner and the outer cores are good electrical conductors. As a result, the inner core rotation ζ_{IC} is enslaved to the fluid angular velocity. Omitting the other torques acting on the inner core in order to focus on this mechanism, we have

$$C_{IC}\frac{\partial \zeta_{IC}}{\partial t} \approx -\Gamma_{M,IC}\left(\zeta_{IC} - \tilde{\zeta}\right) \qquad [127]$$

where C_{IC} is the axial moment of inertia of the solid inner core, and $\tilde{\zeta}$ is some average of the geostrophic velocity within the cylindrical surface tangent to the inner core that depends on the distribution of the radial magnetic field at the ICB. The factor $\Gamma_{M,IC}$ measures the strength of the electromagnetic coupling, and is proportional to the mean-squared value of the radial field at the ICB. Although they consider eqn [127] from a different viewpoint, Roberts and Aurnou (2012) estimate the time response $C_{IC}/\Gamma_{M,IC}$ for a typical 5 mT radial magnetic field at the ICB and find that it is of the order of a few days. As there is little dissipation involved, electromagnetic coupling with the inner core does not hinder the propagation of torsional waves inward as far as the rotation axis (see Figure 2 of Jault and Légaut (2005)).

Electromagnetic coupling of the fluid and solid core also allows an indirect coupling between the fluid core and the mantle, if it operates in parallel with gravitational coupling between the solid inner core and the mantle (see Section 8.09.4.3.2).

A similar mechanism could also operate at the CMB, provided there was sufficient electrical conductivity in the lowermost mantle. In contrast with the situation at the ICB, electromagnetic coupling at the CMB entails attenuation of the torsional waves. Buffett (1998) and Dumberry and Mound (2008) observe that mantle conduction suppresses the torsional waves before they cross the core if the mantle conductance is large enough to make the electromagnetic torque at the CMB contribute significantly to l.o.d. changes.

Roberts and Aurnou (2012) note that frictional coupling between the fluid and the solid cores may also be important for the reason that their interface is rough if solidification of the inner core occurs through dendritic growth (Deguen, 2012).

8.09.5   Future Directions – Consistent Approach to the Earth's Core Dynamics

8.09.5.1   Diffusion of the Geomagnetic Signal Through the Weakly Conducting Mantle

There is growing seismic evidence that the lowermost mantle is chemically and thermally very heterogeneous (e.g., Lay and Garnero, 2011). A host of 3D structures have been revealed. To cite just one example, dome-like hills sitting on the CMB, up to 100 km high, have been recently imaged using seismic data collected by Earthscope's USArray (Sun et al., 2013). The authors argue that these structures are stabilized at the bottom of the mantle by the addition of a small percentage of Fe-rich oxides. The electrical conductivity of FeO is estimated to be about 9×10^4 S m^{-1} at the pressure and temperature of the CMB, which is much higher than those of other rocks of

the deep mantle (Ohta et al., 2012). Lateral variations of the electrical properties of the lowermost mantle are thus to be expected. They will be very difficult to detect from studies based on the analysis of electrical currents induced in the mantle by varying magnetospheric fields (Kuvshinov, 2012); hence, there is strong motivation for trying, instead, to use the varying core field as the source.

Three types of observations may be used to constrain the mantle conductivity from the bottom. First, the time correlation properties of observatory records and of the geomagnetic coefficient series at Earth's surface may provide us with information about the smoothing of the magnetic signal through the conducting mantle (Gillet et al., 2013; Mandea Alexandrescu et al., 1999). Second, observatory records show abrupt changes in the secular variation of the core field. These events are almost, but not fully, simultaneous at Earth's surface (Alexandrescu et al., 1996). The question has thus arisen whether their different times of occurrence at distinct observatories are caused by the conducting mantle acting as a filter on core signals (Nagao et al., 2003; Pinheiro and Jackson, 2008). Third, changes in the geostrophic flow $\mathbf{u}_G$ throughout the core yield variations in core angular momentum, which can be inferred from observed l.o.d. variations. The flow $\mathbf{u}_G$ also causes the magnetic field outside the core to evolve. Differential delays between magnetic and l.o.d. observations may be ascribable to the conducting mantle (Backus, 1983).

Most work on the transmission of the magnetic field from the core to the mantle has involved a perturbation procedure where the small parameter is the frequency of the core signal. The first order theory gives the zero frequency delay time of the mantle τ_1 (Benton and Whaler, 1983). Backus (1983) extended the theory to the second order and calculated the smoothing time of the mantle. Both Benton and Whaler (1983) and Backus (1983) derived τ_1 as a weighted integral of the mantle conductivity, with a weight vanishing linearly at the CMB,

$$\tau_1 = \frac{\mu_0}{2l+1} \int_{r_c}^{r_e} r\sigma(r) \left(1 - \left(\frac{r_c}{r}\right)^{2l+1}\right) \mathrm{d}r \qquad [128]$$

where l is the harmonic degree of the field, σ is the conductivity as a function of radius, and r_e is Earth's radius. The conclusion that the conductivity of the mantle rocks just above the CMB has no influence on the filtering of magnetic signals emanating from the core is drawn directly from the supposedly perfect knowledge of the field at the core surface, whereas the magnetic field at the CMB actually depends on the mantle conductivity.

Considering the conducting mantle as a filter acting on the magnetic field supposedly perfectly known at the core surface has been misleading. We now need to take a step back and to consider the mechanisms behind the production of a magnetic field at the CMB. From coupled models of core dynamics (as discussed in Sections 8.09.2.2.3 and 8.09.3) and mantle induction, it will be possible to calculate different quantities (time evolution of l.o.d., geographical distribution of sudden magnetic field changes, auto-correlation of geomagnetic coefficients series), which are measurable. When such direct models are available, solutions of the associated inverse problem will include information on the mantle conductivity, especially near the CMB.

8.09.5.2   Filtering Through a Stably Stratified Layer Below the CMB

A variety of mechanisms may cause a stratified layer to establish at the CMB. It has been suggested that light elements collect at the top of the core either because they are entrained in coherent blobs from the ICB to the CMB (Moffatt and Loper, 1994) or because they migrate down the pressure gradient in the outer core (e.g., Gubbins and Davies, 2013). As another possibility, there are indications from high pressure experiments that the core is undersaturated in oxygen (Buffett and Seagle, 2010; Frost et al., 2010) and silicon (Tsuno et al., 2013) with respect to the mantle, which may have led to the development of an O- and Si-enriched low-density layer beneath the CMB. In addition, the top of the core may be thermally stratified as suggested by recent theoretical ab initio studies (de Koker et al., 2012; Pozzo et al., 2012, 2013), which have revised upward the thermal conductivity of the core and, thus, the amount of heat conducted upward along the adiabat. If the temperature gradient has fallen below the adiabat, the upper part of the core (or a layer at intermediate depth if thermal conductivity increases with depth rapidly enough) is thermally stratified (Gomi et al., 2013; Gubbins et al., 2004).

There is some seismological evidence for stable stratification of the outermost core. Helffrich and Kaneshima (2010) have argued, using observations of SmKS waveforms, that the material at the top of the core is 5.9% less dense than the liquid 300 km below it. This corresponds to a Brunt–Väisälä frequency N in the range of 0.51–1.03 mHz or a ratio of $2\Omega/N \sim 0.1$ for a possible stable layer beneath the CMB.

The preceding sections have given us the tools to briefly discuss the effect of a strongly stratified layer ($N \gg \Omega$) below the core surface of depth D. Following Takehiro and Lister (2001), we consider that the motions in the stratified layer originate from convective motions in the underlying unstable layer, with frequency ω. As in Section 8.09.2.2.2, we work in a local Cartesian coordinate system, with x the prograde direction and y directed toward the rotation axis. Here, the z-axis is the gravity axis. In this coordinate system, $\mathbf{\Omega} = \Omega_y \mathbf{1}_y + \Omega_z \mathbf{1}_z$. We further assume that the velocity is proportional to $\exp[i(k_x x + k_y y + nz - \omega t)]$. Including rotational effects but otherwise similar to eqn [34] given earlier, Takehiro and Lister obtained the dispersion relation

$$\omega^2 = \frac{N^2\left(k_x^2 + k_y^2\right) + 4\left(n\Omega_z + k_y\Omega_y\right)^2}{k_x^2 + k_y^2 + n^2} \qquad [129]$$

which transforms into eqns [11] and [34] in the limiting cases $N=0$ and $\Omega=0$, respectively. When $\omega \ll \Omega, N$, eqn [129] gives the following equation for n:

$$N^2\left(k_x^2 + k_y^2\right) + 4n^2(\mathbf{\Omega}\cdot\mathbf{1}_r)^2 \sim 0 \qquad [130]$$

This expression yields the imaginary part of n and, finally, the characteristic penetration depth in the direction parallel to the rotation axis, $\delta \sim \left(2\Omega/\sqrt{k_x^2 + k_y^2}N\right)$.

Using the seismological model of Helffrich and Kaneshima (2010) as an example, large length-scale motions with azimuthal wavenumber $m=3$ and lower are predicted to be able to penetrate through the layer, whereas smaller length-scale

features will penetrate less deeply and be attenuated before reaching the CMB.

8.09.6   Final Remarks

Taking into account dynamical effects such as wave motions and restoring forces is helping to resolve several issues concerning the interpretation of geomagnetic data. For example, it is now known that the geostrophic shear $\partial\zeta/\partial s$ at $s=r_c$ is determined by the condition that the magnetic vector is continuous across the CMB. Conversely, away from the core equator, rapid rotation hinders the propagation of Alfvén waves that would eliminate discontinuities in the magnetic field parallel to the CMB. Also, the pressure torque between the core and the mantle cannot be studied independently from the motions that make the pressure change and it is hoped that a consistent model of torsional waves in the presence of CMB topography will soon emerge. Finally, models of induction in the conducting mantle need to be coupled with models of waves in the core or, more generally, of core dynamics, before observations are interpreted in terms of mantle conductivity.

   Rapid rotation is the key actor in the story that has been told in this chapter. Because it rigidifies the motions in the direction parallel to the rotation axis, only products of the magnetic field components averaged along the direction parallel to the rotation axis enter the equations for fast and large-scale dynamics. This scale anisotropy between flow variations parallel and perpendicular to the rotation axis has recently motivated the development of another set of reduced equations for flows in the presence of strong rotation that is less restrictive than quasi-geostrophy (Grooms et al., 2010; Julien et al., 2006). In this model, axial variations are small only on an axial scale equal to the scale in the perpendicular direction. It would be worthwhile to generalize the axially averaged equations presented in Section 8.09.2.2.3 along the same lines.

References

Abarca del Rio R, Gambis D, and Salstein DA (2000) Interannual signals in length of day and atmospheric angular momentum. *Annales Geophysicae* 18: 347–364.

Acheson DJ (1978) Magnetohydrodynamic waves and instabilities in rotating fluids. In: Roberts PH and Soward AM (eds.) *Rotating Fluids in Geophysics*, pp. 315–349. New York: Academic Press.

Alboussière T, Deguen R, and Melzani M (2010) Melting-induced stratification above the Earth's inner core due to convective translation. *Nature* 466: 744–747.

Alexandrescu M, Gibert D, Hulot G, Le Mouël J-L, and Saracco G (1996) Worldwide wavelet analysis of geomagnetic jerks. *Journal of Geophysical Research* 101: 21975–21994.

Anufriev AP, Jones CA, and Soward AM (2005) The Boussinesq and anelastic liquid approximations for convection in the Earth's core. *Physics of the Earth and Planetary Interiors* 152: 163–190.

Aubert J, Labrosse S, and Poitou C (2009) Modelling the palaeo-evolution of the geodynamo. *Geophysical Journal International* 179: 1414–1428.

Backus G (1968) Kinematics of geomagnetic secular variation in a perfectly conducting core. *Philosophical Transactions of the Royal Society of London, Series A* 263: 239–266.

Backus G (1983) Application of mantle filter theory to the magnetic jerk of 1969. *Geophysical Journal of the Royal Astronomical Society* 74: 713–746.

Becker JM and Salmon R (1997) Eddy formation on a continental slope. *Journal of Marine Research* 55: 181–200.

Benton ER and Whaler KA (1983) Rapid diffusion of the poloidal geomagnetic field through the weakly conducting mantle: A perturbation solution. *Geophysical Journal of the Royal Astronomical Society* 75: 77–100.

Bloxham J, Zatman S, and Dumberry M (2002) The origin of geomagnetic jerks. *Nature* 420: 65–68.

Braginsky SI (1970) Torsional magnetohydrodynamic vibrations in the Earth's core and variations in day length. *Geomagnetism and Aeronomy* 10: 1–8.

Braginsky SI and Roberts PH (1995) Equations governing convection in Earth's core and the geodynamo. *Geophysical and Astrophysical Fluid Dynamics* 79: 1–97.

Bryan GH (1889) The waves on a rotating liquid spheroid of finite ellipticity. *Philosophical Transactions of the Royal Society of London, Series A* 180: 187–219.

Buffett BA (1996) Gravitational oscillations in the length of day. *Geophysical Research Letters* 23: 2279–2282.

Buffett BA (1998) Free oscillations in the length of day: Inferences on physical properties near the core–mantle boundary. In: Gurnis M, Wysession ME, Knittle E, and Buffett BA (eds.) *The Core–Mantle Boundary Region*. Geodynamics Series, vol. 28, pp. 153–165. American Geophysical Union.

Buffett BA (2010) Tidal dissipation and the strength of the Earth's internal magnetic field. *Nature* 468: 952–955. http://dx.doi.org/10.1038/nature09463.

Buffett BA, Mound J, and Jackson A (2009) Inversion of torsional oscillations for the structure and dynamics of Earth's core. *Geophysical Journal International* 177: 878–890.

Buffett BA and Seagle CT (2010) Stratification of the top of the core due to chemical interactions with the mantle. *Journal of Geophysical Research* 115: B04407. http://dx.doi.org/10.1029/2009JB006751.

Busse FH (1970) Thermal instabilities in rapidly rotating systems. *Journal of Fluid Mechanics* 44: 441–460.

Busse FH (2002) Convective flows in rapidly rotating spheres and their dynamo action. *Physics of Fluids* 14: 1301–1314.

Busse FH, Dormy E, Simitev RD, and Soward AM (2007) Dynamics of rotating fluids. In: Dormy E and Soward AM (eds.) *Mathematical Aspects of Natural Dynamos*, pp. 119–198. Boca Raton, FL: CRC Press.

Canet E, Fournier A, and Jault D (2009) Forward and adjoint quasi-geostrophic models of the geomagnetic secular variation. *Journal of Geophysical Research* 114: B11101. http://dx.doi.org/10.1029/2008JB006189.

Christensen UR and Aubert J (2006) Scaling properties of convection-driven dynamos in rotating spherical shells and application to planetary magnetic fields. *Geophysical Journal International* 166: 97–114.

Davidson PA (2001) *An Introduction to Magnetohydrodynamics*. Cambridge: Cambridge University Press.

Deguen R (2012) Structure and dynamics of Earth's inner core. *Earth and Planetary Science Letters* 333–334: 211–225.

Deguen R, Alboussiere T, and Cardin Ph (2013) Thermal convection in Earth's inner core with phase changes at its boundary. *Geophysical Journal International* 194: 1310–1334. http://dx.doi.org/10.1093/gji/ggt202.

Diamond PH, Itoh SI, Itoh K, and Silvers LJ (2007) β-Plane MHD turbulence and dissipation in the solar tachocline. In: Hughes DW, Rosner R, and Weiss NO (eds.) *The Solar Tachocline*, pp. 213–240. Cambridge: Cambridge University Press.

Dumberry M and Mound JE (2008) Constraints on core–mantle electromagnetic coupling from torsional oscillation normal modes. *Journal of Geophysical Research* 113: B03102. http://dx.doi.org/10.1029/2007/JB005135.

Fearn DR and Proctor MRE (1992) Magnetostrophic balance in non-axisymmetric, nonstandard dynamo models. *Geophysical and Astrophysical Fluid Dynamics* 67: 117–128.

Finlay C (2007) Alfvén waves. In: Gubbins D and Herrero-Bervera E (eds.) *Encyclopedia of Geomagnetism and Paleomagnetism*, pp. 3–6. New York: Springer.

Finlay CC (2008) Waves in the presence of magnetic fields, rotation and convection. In: Cardin Ph and Cugliandolo LF (eds.) *Dynamos*, pp. 403–450. Amsterdam: Elsevier.

Finlay CC, Dumberry M, Chulliat A, and Pais MA (2010) Short timescale core dynamics: theory and observations. *Space Science Reviews* 155: 177–218.

Finlay CC and Jackson A (2003) Equatorially dominated magnetic field change at the surface of Earth's core. *Science* 300: 2084–2086.

Fournier A, Hulot G, and Jault D (2010) An introduction to data assimilation and predictability in geomagnetism. *Space Science Reviews* 155: 247–291.

Frost DJ, Asahara Y, Rubie DC, et al. (2010) Partitioning of oxygen between the Earth's mantle and core. *Journal of Geophysical Research* 115: B02202. http://dx.doi.org/10.1029JB006302.

Garcia R and Souriau A (2000) Amplitude of the core–mantle boundary topography estimated by stochastic analysis of core phases. *Physics of the Earth and Planetary Interiors* 117: 345–359.

Gillet N, Jault D, Canet E, and Fournier A (2010) Fast torsional waves and strong magnetic field within the Earth's core. *Nature* 465: 74–77.

Gillet N, Jault D, Finlay CC, and Olsen N (2013) Stochastic modelling of the Earth's magnetic field: Inversion for covariances over the observatory era. *Geochemistry, Geophysics, Geosystems* 14: 766–786. http://dx.doi.org/10.1002/ggge.20041.

Gillet N and Jones CA (2006) The quasi-geostrophic model for rapidly rotating spherical convection outside the tangent cylinder. *Journal of Fluid Mechanics* 554: 343–369.

Gillet N, Schaeffer N, and Jault D (2011) Rationale and geophysical evidence for quasi-geostrophic rapid dynamics within the Earth's outer core. *Physics of the Earth and Planetary Interiors* 187: 78–88.

Gomi H, Ohta K, Hirose K, et al. (2013) The high conductivity of iron and thermal evolution of the Earth's core. *Physics of the Earth and Planetary Interiors,* 224: 88–103. http://dx.doi.org/10.1016/j.pepi.2013.07.010.

Greenspan HP (1965) On the general theory of contained rotating fluid motions. *Journal of Fluid Mechanics* 22: 449–462.

Greenspan HP (1968) *The Theory of Rotating Fluids*. Cambridge: Cambridge University Press.

Grooms I, Julien K, Weiss JB, and Knobloch E (2010) Model of convective Taylor columns in rotating Rayleigh–Bénard convection. *Physical Review Letters* 104: 224501.

Gross RS, Fukumori I, Menemenlis D, and Gegout P (2004) Atmospheric and oceanic excitation of length-of-day variations during 1980–2000. *Journal of Geophysical Research* 109: B01406. http://dx.doi.org/10.1029/2003JB002432.

Gubbins D, Alfè D, Masters G, Price GD, and Gillan M (2004) Gross thermodynamics of two-component core convection. *Geophysical Journal International* 157: 1407–1414.

Gubbins D and Davies CJ (2013) The stratified layer at the core–mantle boundary caused by barodiffusion of oxygen, sulphur and silicon. *Physics of the Earth and Planetary Interiors* 215: 21–28.

Gubbins D and Roberts PH (1987) Magnetohydrodynamics of the Earth's core. In: Jacobs JA (ed.). *Geomagnetism*, vol. 2, pp. 1–183. New York: Academic Press.

Helffrich G and Kaneshima S (2010) Outer-core compositional stratification from observed core wave speed profiles. *Nature* 468: 807–810. http://dx.doi.org/10.1038/nature09636.

Hide R (1966) Free hydromagnetic oscillations of the Earth's core and the theory of the geomagnetic secular variation. *Philosophical Transactions of the Royal Society of London, Series A* 259: 615–647.

Jackson A (2003) Intense equatorial flux spots on the surface of the Earth's core. *Nature* 424: 760–763.

Jackson A, Bloxham J, and Gubbins D (1993) Time-dependent flow at the core surface and conservation of angular momentum in the coupled core–mantle system. In: Le Mouël J-L, Smylie DE, and Herring T (eds.) *Dynamics of Earth's Deep Interior and Earth Rotation*, pp. 97–107. American Geophysical Union.

Jackson A, Jonkers A, and Walker M (2000) Four centuries of geomagnetic secular variation from historical records. *Philosophical Transactions of the Royal Society of London, Series A* 358: 957–990.

Jault D (2003) Electromagnetic and topographic coupling, and LOD variations. In: Jones CA, Soward AM, and Zhang K (eds.) *Earth's Core and Lower Mantle*, pp. 55–76. Boca Raton, FL: CRC Press.

Jault D (2008) Axial invariance of rapidly varying diffusionless motions in the Earth's core interior. *Physics of the Earth and Planetary Interiors* 166: 67–76.

Jault D, Gire C, and Le Mouël J-L (1988) Westward drift, core motions and exchanges of angular momentum between core and mantle. *Nature* 333: 353–356.

Jault D and Légaut G (2005) Alfvén waves within the Earth's core. In: Soward AM, Jones CA, Hughes DW, and Weiss NO (eds.) *Fluid Dynamics and Dynamos in Astrophysics and Geophysics*, pp. 277–293. Boca Raton, FL: CRC Press.

Julien K, Knobloch E, Milliff R, and Werne J (2006) Generalized quasi-geostrophy for spatially anisotropic rotationally constrained flows. *Journal of Fluid Mechanics* 555: 233–274.

Koelemeijer PJ, Deuss A, and Trampert J (2012) Normal mode sensitivity to Earth's D″ layer and topography on the core–mantle boundary: What we can and cannot see. *Geophysical Journal International* 190: 553–568.

de Koker N, Steinle-Neumann G, and Vlček V (2012) Electrical resistivity and thermal conductivity of liquid Fe alloys at high P and T, and heat flux in Earth's core. *Proceedings of the National Academy of Sciences* 109: 4070–4073.

Koper KD, Pyle ML, and Franks JM (2003) Constraints on aspherical core structure from PKiKP-PcP differential travel times. *Journal of Geophysical Research* 108: 2168. http://dx.doi.org/10.1029/2002JB001995.

Kudlick MD (1966) *On Transient Motions in a Contained Rotating Fluid*. Ph.D. Thesis, Massachussets Institute of Technology, Mathematical Department.

Kuvshinov A (2012) Deep electromagnetic studies from land, sea, and space: Progress status in the past 10 years. *Surveys in Geophysics* 33: 169–209.

Labrosse S, Poirier J-P, and Le Mouël J-L (2001) The age of the inner core. *Earth and Planetary Science Letters* 190: 111–123.

Lassak T, McNamara A, Garnero E, and Zhong S (2010) Core–mantle boundary topography as a possible constraint on lower mantle chemistry and dynamics. *Earth and Planetary Science Letters* 289: 232–241.

Lay T and Garnero E (2011) Deep mantle seismic modeling and imaging. *Annual Review of Earth and Planetary Sciences* 39: 91–123.

Lehnert B (1954) Magnetohydrodynamic waves under the action of the coriolis force. *The Astrophysical Journal* 119: 647–654.

Mandea Alexandrescu M, Gibert D, Le Mouël J-L, Hulot G, and Saracco G (1999) An estimate of average lower mantle conductivity by wavelet analysis of geomagnetic jerks. *Journal of Geophysical Research* 104: 17735–17745.

Mathews PM, Buffett BA, Herring TA, and Shapiro II (1991) Forced nutations of the Earth: Influence of inner core dynamics: 2. Numerical results and comparisons. *Journal of Geophysical Research* 96: 8243–8257.

Mathews PM, Herring TA, and Buffett BA (2002) Modeling of nutation and precession: New nutation series for nonrigid Earth and insights into the Earth's interior. *Journal of Geophysical Research* 107: 2068. http://dx.doi.org/10.1029/2001JB000390.

Mizzon H and Monnereau M (2013) Implication of the lopsided growth for the viscosity of Earth's inner core. *Earth and Planetary Science Letters* 361: 391–401.

Moffatt K and Loper DE (1994) The magnetostrophic rise of a buoyant parcel in the Earth's core. *Geophysical Journal International* 117: 394–402.

Monnereau M, Calvet M, Margerin L, and Souriau A (2010) Lopsided growth of Earth's inner core. *Science* 328: 1014–1017.

Morse PM and Feshbach H (1953) *Methods of Theoretical Physics*. Part I, New York: McGraw-Hill.

Mound JE and Buffett BA (2005) Mechanisms of core–mantle angular momentum exchange and the observed spectral properties of torsional oscillations. *Journal of Geophysical Research* 110: B08103. http://dx.doi.org/10.1029/2004JB003555.

Mound JE and Buffett BA (2006) Detection of a gravitational oscillation in length-of-day. *Earth and Planetary Science Letters* 243: 383–389.

Nagao H, Iyemori T, Higuchi T, and Araki T (2003) Lower mantle conductivity anomalies estimated from geomagnetic jerks. *Journal of Geophysical Research* 108. http://dx.doi.org/10.1029/2002JB001786.

Ohta K, Cohen RE, Hirose K, Haule K, Shimizu K, and Ohishi Y (2012) Experimental and theoretical evidence for pressure-induced metallization in FeO with rocksalt-type structure. *Physical Review Letters* 108: 026403.

Pais MA and Jault D (2008) Quasi-geostrophic flows responsible for the secular variation of the Earth's magnetic field. *Geophysical Journal International* 173: 421–443.

Pinheiro K and Jackson A (2008) Can a 1-D mantle electrical conductivity model generate magnetic jerk differential time delays? *Geophysical Journal International* 173: 781–792.

Plaut E and Busse FH (2002) Low-Prandtl-number convection in a rotating cylindrical annulus. *Journal of Fluid Mechanics* 464: 345–363.

Poirier J-P and Tarantola A (1998) A logarithmic equation of state. *Physics of the Earth and Planetary Interiors* 109: 1–8.

Pozzo M, Davies C, Gubbins D, and Alfè D (2012) Thermal and electrical conductivity of iron at Earth's core conditions. *Nature* 485: 355–358. http://dx.doi.org/10.1038/nature11031.

Pozzo M, Davies C, Gubbins D, and Alfè D (2013) Transport properties for liquid silicon–oxygen–iron mixtures at Earth's core conditions. *Physical Review B* 87: 014110.

Rieutord M and Dintrans B (2002) More concerning the anelastic and subseismic approximations for low-frequency modes in stars. *Monthly Notices of the Royal Astronomical Society* 337: 1087–1090.

Rieutord M, Georgeot B, and Valdetarro L (2001) Inertial waves in a rotating spherical shell: Attractors and asymptotic spectrum. *Journal of Fluid Mechanics* 435: 103–144.

Roberts PH and Aurnou JM (2012) On the theory of core–mantle coupling. *Geophysical and Astrophysical Fluid Dynamics* 106: 157–230. http://dx.doi.org/10.1080/03091929.2011.589028.

Roberts PH and King EM (2013) On the genesis of the Earth's magnetism. *Reports on Progress in Physics* 76: 096801.

Roberts PH and Scott S (1965) On analysis of the secular variation 1. A hydrodynamic constraint: Theory. *Journal of Geomagnetism and Geoelectricity* 17: 137–151.

Roberts PH and Soward AM (1972) Magnetohydrodynamics of the Earth's core. *Annual Review of Fluid Mechanics* 4: 117–154.

Roberts PH, Yu ZJ, and Russell CT (2007) On the 60-year signal from the core. *Geophysical and Astrophysical Fluid Dynamics* 101: 11–35.

Schaeffer N and Cardin Ph (2005) Quasi-geostrophic model of the instabilities of the Stewartson layer in flat and depth-varying containers. *Physics of Fluids* 17: 104111.

Schaeffer N, Jault D, Cardin Ph, and Drouard M (2012) On the reflection of Alfvén waves and its implication for Earth's core modelling. *Geophysical Journal International* 191: 508–516.

Silva L, Jackson L, and Mound J (2012) Assessing the importance and expression of the 6 year geomagnetic oscillation. *Journal of Geophysical Research* 117: B10101, http://dx.doi.org/10.1029/2012JB009405.

Simmons NA, Forte AM, Boschi L, and Grand SP (2010) Gypsum: A joint tomographic model of mantle density and seismic wave speeds. *Journal of Geophysical Research* 115: B12310. http://dx.doi.org/10.1029/2010JB007631.

Smylie DE, Szeto AMK, and Rochester MG (1984) The dynamics of the Earth's inner and outer cores. *Reports on Progress in Physics* 47: 855–906.

Soldati G, Boschi L, and Forte AM (2012) Tomography of core–mantle boundary and lowermost mantle coupled by geodynamics. *Geophysical Journal International* 189: 730–746.

Soward AM and Roberts PH (2007) Taylor's constraint. In: Dormy E and Soward AM (eds.) *Mathematical Aspects of Natural Dynamos*, pp. 419–424. Boca Raton, FL: CRC Press.

Staplehurst PJ, Davidson PA, and Dalziel SB (2008) Structure formation in homogeneous freely decaying rotating turbulence. *Journal of Fluid Mechanics* 598: 81–105.

Stewartson K (1957) The dispersion of a current on the surface of a highly conducting fluid. *Mathematical Proceedings of the Cambridge Philosophical Society* 53: 774–775.

Sun D, Helmberger DV, Jackson JM, Clayton RW, and Bower DJ (2013) Rolling hills on the core–mantle boundary. *Earth and Planetary Science Letters* 361: 333–342.

Sze EKM and van der Hilst RD (2003) Core mantle boundary topography from short period PcP, PKP, and PKKP data. *Physics of the Earth and Planetary Interiors* 135: 27–46.

Takehiro S and Lister JR (2001) Penetration of columnar convection into an outer stably stratified layer in rapidly rotating spherical fluid shells. *Earth and Planetary Sciences Letters* 187: 357–366.

Taylor GI (1923) Experiments on the motion of solid bodies in rotating fluids. *Proceedings of the Royal Society of London A* 104: 213–218.

Taylor JB (1963) The magneto-hydrodynamics of a rotating fluid and the Earth's dynamo problem. *Proceedings of the Royal Society of London* A274: 274–283.

Tobias S, Hughes DW, and Diamond PH (2007) β-Plane magnetohydrodynamic turbulence in the solar tachocline. *The Astrophysical Journal* 667: L113–L116.

Tsuno K, Frost DJ, and Rubie DC (2013) Simultaneous partitioning of silicon and oxygen into the Earth's core during early Earth differentiation. *Geophysical Research Letters* 40: 66–71. http://dx.doi.org/10.1029/2012GL054116.

Vallis GK (2006) *Atmospheric and Oceanic Fluid Dynamics: Fundamentals and Large-Scale Circulation*. Cambridge: Cambridge University Press.

Yoshida M (2008) Core–mantle boundary topography estimated from numerical simulations of instantaneous mantle flow. *Geochemistry, Geophysics, Geosystems* 9: Q07002. http://dx.doi.org/10.1029/2008GC002008.

Zatman S and Bloxham J (1997) Torsional oscillations and the magnetic field within the Earth's core. *Nature* 388: 760–763.

Zhang K, Earnshaw P, Liao X, and Busse FH (2001) On inertial waves in a rotating fluid sphere. *Journal of Fluid Mechanics* 437: 103–119.